Shahid Bahonar University of Kerman
Agricultural Biotechnology Journal
Iranian Biotechnology Society
Print ISSN: 2228-6705 Online ISSN: 2228-6500

Experimental and In Silico evaluation of a novel ZnO/Alhagi maurorum/PVA composite film against multidrug-resistant *Pseudomonas aeruginosa* harboring *blaTEM* and *blaIMP* genes

Nisreen Kaddim Radi
* Corresponding author. Department of Biology, College of Science for Women, University of Babylon, Iraq. E-mail: nesreenzain.83@gmail.com and Nasreen.radi@uobabylon.edu.iq

Shireen Sabah Kamil
Department of Biology, College of science for women, University of Babylon, Iraq. E-mail: Shireensbahkamil@gmail.com

Safa Hasan Radhi
Biology Department, College of science, Al-Qasim Green University, Babylon 51013, Iraq. E-mail: safa.safa252016@gmail.com

Hussein J. Hussein
Department of Biology, College of science for women, University of Babylon, Iraq. E-mail: huss2010feb@yahoo.com

Ali H. Al-Marzoqi
Department of Biology, College of science for women, University of Babylon, Iraq. E-mail: almarzoqiali80@gmail.com

Lubna Abdulazeem
DNA Research center, University of Babylon, Iraq. E-mail: sci.lubna.addeladeem@uobabylon.edu.iq

Israa A. Ibraheam
Department of Biology, College of science for women, University of Babylon, Iraq. E-mail: israaibraheam2016@gmail.com

Ali Salam Kashkool
Middle Technical University, Kut Technical Institute, Iraq. E-mail: alimayhie11@gmail.com

Abstract

Objective

A major contributor to burn infections, *Pseudomonas aeruginosa* is known for its aggressiveness and medication resistance. This study was carried out to prepare and characterize ZnONPs/PVA (nanoparticles) film loaded with *Alhagi maurorum* extract for multidrug-resistant *Pseudomonas aeruginosa* isolated from skin burn infections, as well as to molecularly detect and sequence *blaTEM* and *blaIMP* genes followed by an in-silico docking analysis to investigate the antibacterial mechanism.

Materials and methods

Alhagi maurorum shoots were collected. Voucher specimens were retained. The GC-MS analysis was performed. Zinc oxide nanoparticles (ZnO-NPs) were used in the polymer matrix. Comprehensive assessments were conducted to demonstrate the successful entrapment and homogeneous distribution of bioactivating nanocomponents in the polymeric matrix of the fabricated composite film. Fifty bacterial isolates were obtained from burn swabs that had been isolated from the burn unit at AL-Sadiq Teaching Hospital, Babylon, Iraq. The antimicrobial susceptibility of *P. aeruginosa* isolates (n = 20) was determined. Genomic DNA from bacterial isolates was isolated and PCR was performed. The nucleotide sequences of the *blaTEM* gene from *P. aeruginosa* were acquired from the National Center for Biotechnology Information (NCBI). SPSS software was used for statistical analysis.

Results

GC-MS revealed that the mass spectrum and structure of twelve chemical components extracted from *Alhagi maurorum* using methanol are displayed in the GC-MS data. Among them, 9,12-Octadecadienoic acid (Z,Z)-(Linoleic) was unique. By incorporating these phytochemicals into a PVA polymer matrix with zinc nanoparticles, we created a film that decomposes naturally. The film was tested against medical isolates of Pseudomonas aeruginosa, which are drug-resistant bacteria. Among 50 bacterial isolates, 20 were identified as P. aeruginosa. PCR analysis revealed the presence of *blaTEM* and *blaIMP* genes in a substantial proportion of the isolates. Molecular docking results suggest that the ZnO nanostructure has the highest binding potential toward the 4b7q protein compared to linoleic acid and PVA. The strong binding affinity and low inhibition constant of ZnO highlight its potential role as a stable binder or inhibitor, whereas linoleic acid and PVA are less effective.

Conclusion: The strong antibacterial properties of the composite film are probably the result of the PVA polymer, zinc nanoparticles, and plant extract working in concert. The ZnO/Alhagi/PVA composite film demonstrated promising antibacterial and antioxidant activities and may represent a potential biodegradable wound-dressing material for managing MDR *P. aeruginosa* infections.

Keywords: *Alhagi marorum,* antibacterial films, beta-lactamase, polyvinyl alcohol, zinc nanoparticles

Paper Type: Research Paper.

Citation: Radi, N. K., Kamil, S. S., Radhi, S. H., Hussein, H. J., Al-Marzoqi, A. H., Abdulazeem, L., & Kashkool, A. S. (2026). Experimental and In Silico evaluation of a novel ZnO/Alhagi maurorum/PVA composite film against multidrug-resistant *Pseudomonas aeruginosa* harboring *blaTEM* and *blaIMP* genes. *Agricultural Biotechnology Journal,* 18(4), 339-372.

Agricultural Biotechnology Journal, 18(4), 339-372. DOI: 10.22103/jab.2026.27227.1909

Received: April 13, 2026. Received in revised form: June 19, 2026.

Accepted: June 20, 2026. Published online: August 30, 2026.

Publisher: Shahid Bahonar University of Kerman & Iranian Biotechnology Society.

Introduction

Burn injuries are one of the important health care challenges in low- and middle-income countries, where there is a lack of resources for advanced wound care. Thermal trauma

compromises the skin barrier, providing a nutrient-rich and moist habitat ideal for microbial colonization and infection, leading to impaired healing, sepsis, and mortality. Burn wound infections are one of the major causes of prolonged hospital stays and high treatment costs globally (Ghasemi et al., 2025). *Pseudomonas aeruginosa* is widely considered adaptable, opportunistic, and intrinsically resistant to many classes of antibiotics amongst usual burn wound pathogens. In particular, its ability to colonize and survive under hostile environmental conditions makes it one of the leading contributors to burn-associated infections (Tacconelli et al., 2018). In Iraqi healthcare systems mainly, the profile of resistance continues to develop (Ibrahim et al., 2021), and multidrug-resistant (MDR) *P. aeruginosa* has posed an additional challenge for clinical management. Among the most prominent mechanisms of resistance is the production of β-lactamase enzymes, which inactivate important β-lactam antibiotics, including extended-spectrum β-lactamases (ESBLs). Among these resistance determinants, *blaTEM* is one of the most frequently reported genes. This gene is widely associated with resistance and horizontal transfer; hence, it is a significant driver for molecular surveillance (Oliver et al., 2025). The growing incidence of MDR pathogens together with restrictions on standard antibiotic therapy makes clear the need for alternative economic and accessible therapy. This has led to the emergence of polymeric platforms for wound dressings that offer structural integrity as well as antimicrobial activity, which have been investigated for next-generation therapeutic applications. Polyvinyl alcohol (PVA) is a well-known biomedical polymer that, due to being biocompatible, non-toxic, hydrophilic, and with good film-forming ability, makes it a good candidate for wound dressing applications (Liang et al., 2024). On the other hand, nanotechnology is a multidisciplinary scientific field that uses a set of tools and techniques derived from engineering, physics, chemistry and biology (Heidarpour et al. 2011). Advances in nanoscience and nanotechnology have routinely enabled the fabrication and identification of submicron bioactive carriers. The delivery of bioactive substances to target sites in the body and their release behavior are directly affected by particle size. Compared to micrometer-sized carriers, nanocarriers provide more surface area and have the potential to increase solubility, increase bioavailability, improve controlled release, and enable precise targeting of entrapped substances (Zarrabi et al., 2020). Zinc oxide nanoparticles (ZnO NPs) have strong, wide-spectrum antibacterial activity arising from mechanisms including reactive oxygen species production, membrane damage, and binding with intracellular components (Franco et al., 2022). These features render ZnO NPs fascinating additives for composite films targeted toward controlling MDR bacterial infections. Concurrently, natural plant extracts are an inexpensive source of bioactive compounds. As for one example, *Alhagi maurorum* (a plant widely growing in Iraq) is known to contain some phytochemicals with proven antibacterial activity (Al-Snafi, 2015). Recently integrated studies revealed the possibility of combining polymeric matrices with biologically active plant extracts and further agents to form materials with superior biologic performance. For example, Hussein et al. (2025) discussed the synergistic computational and experimental investigation of propolis, PVA, and *Alhagi maurorum* with promising anticancer and antibacterial activity, illustrating the potential of adding natural extracts to polymer and nanoparticle systems.Molecular docking analyses further provide mechanistic information on the binding of bioactive compounds with antimicrobial resistance-

related target proteins in conjunction with empirical evaluations. Several in silico modeling studies have shown that exploratory applications help in determining predicted binding affinities, which could rationalize functional inhibitory effects of certain molecules leading to observed antibacterial activity on a molecular level (Jabalia et al., 2021). The current study focuses on developing and characterizing a promising antibacterial biodegradable film containing PVA, *Alhagi maurorum* extract, and ZnO nanoparticles that may be used as an alternative therapeutic strategy for MDR *P. aeruginosa* isolated from burn patients in Babylon Governorate/Iraq. Moreover, this study also comprises molecular docking analysis to explore the interactions of selected bioactive compounds with targets associated with resistance and to provide a mechanistic insight into the experimental observations.

Material and methods

Plant collection and extraction: We collected *Alhagi maurorum* shoots from their native habitats in the Babylon Governorate of Iraq during the blossoming season. The plant was taxonomically identified, and voucher specimens were retained. It was washed, air-dried in the shade at room temperature, and then ground into a fine powder. Five hundred mL of 95% methanol was then added, and the mixture was left at room temperature for 72 h with the powdered material coming into contact with the solvent. The dry methanolic extract was prepared by filtration and concentration of the filtrates at 40°C using a rotary evaporator. Then it was stored at 4°C until the time of use for GC-MS analysis and film preparation. Conventional methods of phytochemical extraction were used (Hussein et al., 2025*)*.

GC mass analysis: The GC-MS analysis was repeated with samples from the same plant and blank samples to confirm that the detected chemical is natural. The chemical appeared consistently in all plant samples and disappeared completely in blank samples, proving it is a plant product and not contamination. Alhagi maurorum's dried methanolic extract was analyzed for phytochemicals using gas chromatography-mass spectrometry (GC-MS). The analysis was done using a gas chromatography system along with a mass spectrometer, like those from Agilent Technologies, and helium was used as the carrier gas. To identify substances, we compared their mass spectra with the ones in the NIST library database using methods that had already been established (Saber et al., 2022*)*.

Zinc oxide nanoparticles Dispersion: Zinc oxide nanoparticles (ZnO-NPs) provided by US Research Nanomaterials, Inc. (USA) were used in the polymer matrix according to a dispersion protocol applied to achieve homogeneity and minimum agglomeration. The nanoparticles were measured based on the desired loading percentage (1-5% w/w with respect to polymer) and dispersed in a small volume of solvent (deionized water). Ultrasonicating for 20-30 min was done to obtain uniform dispersion and disrupt the aggregates. The so-obtained suspension was slowly added to the polymer solution with continuous stirring, and mixing continued for 1-2 hours, ensuring homogeneous ZnO-NP distribution in the matrix (Wong et al., 2025*)*.

Films formation: Granular materials of Iran's Amir Kabir Petrochemical Company polyvinyl alcohol (PVA). As indicated by Table 1, four groups of samples are prepared. Following the dissolution of 2 grams of polyvinyl alcohol in 40 milliliters of distilled water, the solution is

heated on a hot plate stirrer at a temperature of 70 degrees Celsius for two hours to prepare a pure polyvinyl alcohol solution (PVA). In contrast, the other groups are prepared accordingly. Once the pure polymer had dissolved after the procedure above, and the PVA powder had developed a thick solution. 4 milliliters of *Alhagi maurorum* extract and ZnO nanoparticles were sequentially added to the mixture of the PVA. The solution was stirred without the use of heat until the solution homogenized. Next step: spread the solutions onto a 25 x 25 cm petri dish and allow to dry at room temperature for 48 hours. Lastly, the films that had been created were peeled and analyzed (Table 1).

Table 1. Film preparation

No.	Sample name	Weight fraction of polymer PVA wt.%	*Alhagi maurorum* extract mL	ZnO nps (%wt)	The Films after dried and cuts
1	PVA+ZnO	100%	0	4	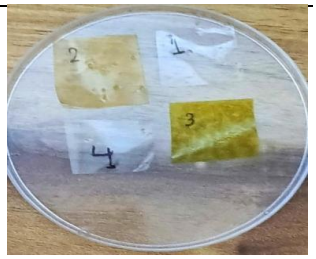
2	PVA+Extract	100%	4	0	
3	PVA+Extract+ZnONPs	100%	2	2	
4.	Pure polymer	100%	0	0	

Nano characterization of ZnO/Alhagi/PVA films: Comprehensive assessments were conducted to demonstrate the successful entrapment and homogeneous distribution of bioactivating nanocomponents in the polymeric matrix of the fabricated composite film. Surface morphology was evaluated using field-emission scanning electron microscopy (FE-SEM). It described a uniform, dense surface morphology featuring evenly distributed nanoscale plateaus with no appreciable phase segregation in the polymer system, indicating that both the nanoparticle and polymeric backbone were strongly interfacial compatible. Particles had an average size in the nanometric scale, estimated through high-resolution micrographs, allowing for efficient integration of particles at the nano level (Brzęk & Sterzyński, 2020). X-ray diffraction (XRD) analysis showed typical crystalline reflections ascribed to the encapsulated nanoparticles, and the polymer matrix was still semi-crystalline, indicating structural stability without significant disruption of the host network. The intermolecular interactions likely hydrogen bonding and electrostatic interactions between the polymer chains and bioactive constituents were also further supported, as depicted by slight peak moves and intensity changes, via Fourier transform infrared spectroscopy (FTIR). Together, these nanochemical and structural analyses demonstrate the successful fabrication of a stable integrated nanocomposite film that is well suited for advanced biomedical applications where nanodistribution and functional performance determinable by structure are required (Brzęk & Sterzyński, 2020).

***Pseudomonas aeruginosa* isolation and detection:** Fifty bacterial isolates were obtained from burn swabs that had been isolated from the burn unit at AL-Sadiq Teaching

Hospital, Babylon, Iraq, between January 2024 and March 2025. The isolates were grown on MacConkey agar and cetrimide agar, and then they were incubated for 24 hours at 37°C. Colonies were detected utilizing morphological, biochemical, and developmental features on selective media. The VITEK® 2 compact system (bioMérieux, France) was employed for final validation as instructed by the manufacturer (Hakeem et al., 2024).

AST profile: The antimicrobial susceptibility of *P. aeruginosa* isolates (n = 20) was determined using the VITEK automated system. Out of the 20 tested isolates, all 20 (100%) showed resistance patterns similar to extensively drug-resistant (XDR) bacteria and met the requirements to be classified as multidrug-resistant (MDR) according to Hakeem et al. (2024).

Antibacterial test: The agar diffusion method was used to test how well the ZnO/Alhagi/PVA composite films can fight bacteria. Sterile Mueller-Hinton agar plates were inoculated with standardized *P. aeruginosa* suspensions (adjusted to 0.5 McFarland). The manufactured films were cut into 1×1 cm squares and put onto inoculated agar plates. The antibacterial activity was measured using a digital caliper after 24 hours of incubation at 37°C by measuring the clear zone of inhibition (ZOI) that emerged from the edges of square films (Abdulbary, 2019).

Antioxidant activity test: The DPPH radical cation method (2,2-diphenyl-1-picrylhydrazyl) was changed to test how well 100 pure chemical compounds can neutralize free radicals. The DPPH reagent (8 mg) was dissolved in 100 mL of MeOH to achieve the desired solution concentration. The concentration was set at 80 mg/mL. To test the scavenging activity, combine 100 µg of DPPH reagent with 100 µg of sample in a 96-well microplate and incubate at room temperature for 30 minutes. After incubation, absorbance was measured at 514 nm using an ELISA reader (TECAN, Groding, Austria), with 100% methanol as a control. The DPPH scavenging effect was calculated with the following formula: Radical scavenging = [(A_control − A_sample) / A_control] × 100. The IC50 DPPH values (the sample concentration required to block 50% of DPPH radicals) were extrapolated from regression analysis. The antioxidant was tested based on its IC50 value (Gulcin & Alwasel, 2023).

Beta-lactamase gene detection of *P. aeruginosa:* *Aeruginosa* bacteria were tested for *blaTEM* and blaIMP-1 from wound patients. For confirmation, traditional microbiological tests such as Gram staining, morphological features, and biochemical assays were performed. Genomic DNA from bacterial isolates was isolated using a kit. Genomic DNA was measured using electrophoresis and the Magician Nano spectrophotometer at A260/A280 and A260/A230 ratios. Conventional PCR amplified virulence genes. utilized PCR primers (Table 2). The gene gradient PCR reaction was made by mixing 4 µL of template DNA, 10 µL of master mix, and 3 µL of forward and reverse primer. for the *blaIMP* gene began with an initial denaturation step at 94°C for 2 minutes, which was performed once. was followed by 30 amplification cycles, each consisting of a denaturation step at 95°C for 1 minute, an annealing step at 55°C for 1 minute, and an extension step at 72°C for 1.5 minutes. After completing the cycles, a final extension step was carried out at 72°C for 5 minutes. Finally, the reaction mixture was held at 4°C for storage. In contrast, the PCR conditions for the *blaTEM* gene started with a single initial denaturation at 95°C for 2 minutes. This was followed by 30 cycles. The reaction included denaturation at 95°C

for 1 minute, followed by annealing at 58°C for 1 minute, and extension at 72°C for 1.5 minutes, with a final extension at 72°C for 5 minutes before being held at 4°C for storage. The PCR mixture consisted of 4 µL of DNA, 10 µL of master mix, 2 forward primers, and 2 reverse primers. Total reaction volume was adjusted to 20 µL using nuclease-free water. PCR products were analyzed on 1.5% agarose and recolored with 5 µg/mL RedSafe nucleotide base stain (Nandy et al., 2017; Radi & Al-Marzoqi, 2022)

Table 2. Characteristics of used primers in the current study

Genes for Paerogino sa	Primers		Product size (bp)	Ref.
	forward	Reverse		
bla $_{TEM}$	TTAGACGTCAGGTGGC ACTT	GGACCGGAGTTACCAA TGCT	972	Radi & Al-Marzoqi (2022)
bla $_{IMP-1}$	CAGATTGCCGATGGTG TTTGG	AGGTGGGCCATTCAGC CAGA	380	Nandy et al. (2017)

Gene sequencing and phylogenetic analysis: The nucleotide sequences of the *blaTEM* gene from *P. aeruginosa* were acquired from the National Center for Biotechnology Information (NCBI). The *blaTEM* sequence was obtained. Sequences had been described previously in clinically isolated *P. aeruginosa* strains conferring β-lactam resistance. Sequences were downloaded in FASTA format for further molecular assessment.

Statistical analysis: SPSS version 22 with the precise test package (IBM, USA) was used for statistical analysis. The chi-square test was used to compare isolate variables; having a p-value of 0.05 or less was deemed statistically significant.

Results

The process of analysis with gas chromatography and mass spectroscopy for detection of the phytochemical compounds was approved in the methanolic extract of the *Alhagi maurorum* shoot part. According to the GC-MS spectrum, the results revealed that twelve phytochemical compounds were detected in the methanolic extract of the *Alhagi maurorum* shoot part (Table 3). The results of the current study uncovered that the first one of these compounds is 1-(2-phenyl-1, 3, 2-dioxaborolan-4-yl)-1, 2-ethanediol (Figure 1). Retention time was 2.041/min (Table 1), and the second phytochemical compound detected was methoxy(n-pentyloxy)methylsilane. In addition to the detection of the following phytochemical compounds, such as toluene (Figure 1), phthalic acid , trimethyl(n-pentyl)silane, 7,8-Diazabicyclo[4.2.0]octane, 1-methyl-, 7,8-dioxide, 13-methyltetradec-9-enoic acid methyl ester , 1,1'-bicyclopropyl, 2-amino-2-oxoethyl acetate , 9,12-octadecadienoic acid (Z,Z)- , 2,4-pentadienoic acid, 1-cyclopenten-3-on-1-yl ester, and 1-butyne, 3,3-dimethyl- . Finally, in one hand, compounds such as 1-(2-phenyl-1,3,2-dioxaborolan-4-yl)-1,2-ethanediol, phthalic acid, diazabicyclo[4.2.0]octane, 1-methyl-7,8-dioxide, 13-methyltetradec-9-enoic acid methyl ester, 2-amino-2-oxoethyl acetate, 9,12-octadecadienoic acid (Z,Z), and 2,4-pentadienoic acid, 1-cyclopenten-3-on-1-yl ester showed potential antibacterial and antifungal activity based on chemical structure. On the other hand, compounds like methoxy (n-pentyloxy) methylsilane, toluene, trimethyl (n-pentyl) silane, 1, 1'-bicyclopropyl, and 1-

butyne, 3, 3-dimethyl, have no significant biological activity. Along with the major bioactive compounds we discussed, the all-inclusive GC-MS report detected more secondary metabolites. (as detailed in the attached Supplementary Report, including mass spectra of all detected peaks and library matching (NIST/Wiley) (Figure 1, Table 3). The GC-MS chromatogram of *Alhagi maurorum* ethanolic extract is shown in Figure 1. Retention times and identification of the major compounds are presented in Table 3.

Table 3. Phytochemical compounds detected in the shoot part of *Alhagi maurorum* using the GC-Mass technique

Peak No.	Compound name	Retention time/min	Molecular formula	Molecular weight g/mole	Peak%	Reported biological activities (based on literature)	Probability %
1	1-(2-Phenyl-1,3,2-dioxaborolan-4-yl)-1,2-ethanediol	2.041	$C_{10}H_{13}BO_4$	208	2.29	Antibacterial and Antifungal	65
1	Methoxy(n-pentyloxy)methylsilane	2.261	$C_7H_{18}O_2Si$	162	34.45	Used in combination of antimicrobial agent	62
2	Toluene	13.817	C_7H_8	92	0.86	Toxic	94
3	Phthalic acid	18.064	$C_{15}H_{20}O_4$	264	2.79	Antibacterial and Antifungal	85
4	Trimethyl(n-pentyl)silane	19.339	$C_8H_{20}Si$	144	1.39	Used in organic synthesis	66
5	7,8-Diazabicyclo[4.2.0]octane, 1-methyl-, 7,8-dioxide	19.396	$C_7H_{12}N_2O_2$	156	6.20	Antibacterial and Antifungal	76
6	13-Methyltetradec-9-enoic acid methyl ester	19.461	$C_{16}H_{30}O_2$	254	0.47	Antibacterial and Antifungal	74
7	1,1'-Bicyclopropyl	19.619	C_6H_{10}	82	0.33	Limited evidence of biological activity	83
8	2-Amino-2-oxoethyl acetate	19.917	$C_4H_7NO_3$	117	42.42	Antibacterial and Antifungal	81
9	9,12-Octadecadienoic acid (Z,Z)-(Linoleic)	22.813	$C_{18}H_{32}O_2$	280	0.57	Antibacterial and Antifungal	80
10	2,4-Pentadienoic acid, 1-cyclopenten-3-on-1-yl ester	23.419	$C_{10}H_{10}O_3$	178	0.61	Antibacterial and Antifungal	90
11	1-Butyne, 3,3-dimethyl-	25.238	C_6H_{10}	82	7.63	Limited evidence of biological activity	87

Characterization of nanoparticles: The four film formulations were evaluated for optical properties by recording the UV-Vis absorption spectra (Figure 2). Pure PVA (Figure 2d) showed very little absorption in the UV-visible range. The distinct absorption bands are attributed to ZnO NPs + PVA (Figure 2a) and PVA + Alhagi extract (Figure 2b). The ZnO/PVA-Alhagi

nanocomposite (Figure 2c), most importantly, revealed a bimetallic absorption pattern, where the characteristic peaks of both metallic and botanical-resource counterparts coexist.

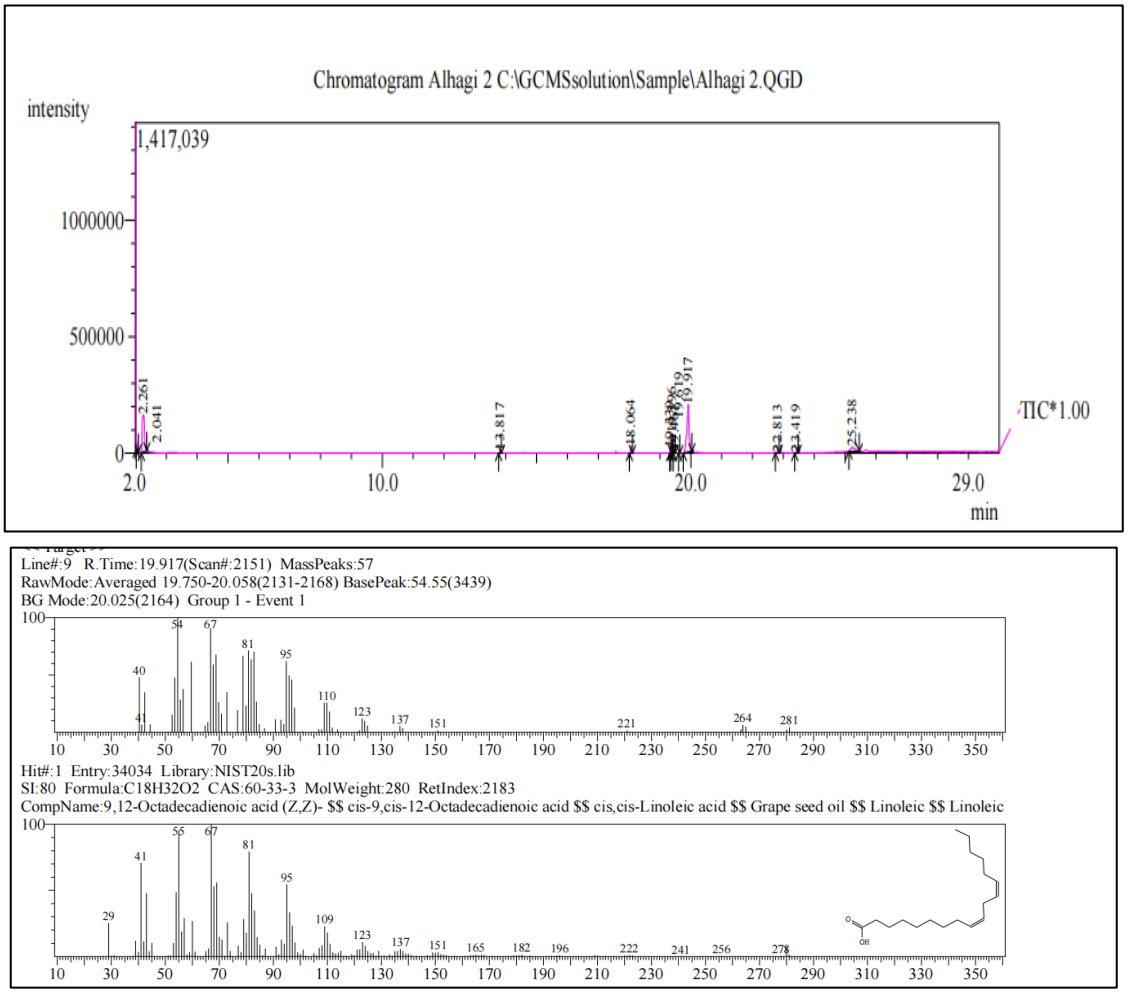

Figure 1. (a) GC-MS chromatogram of *Alhagi maurorum* ethanolic extract. Peaks and their retention times provide an insight about the composition of different compounds in extract. (b) GC-MS analysis of ethanolic extract of *Alhagi maurorum* showing the prominent peak at retention index 2183. The identified compound was linoleic acid (9,12-octadecadienoic acid (Z,Z)) with a molecular weight of 280 g/mol and a formula of C18_H32-O2. The identification revealed a high similarity index (SI:80) with respect to the NIST20s.lib reference database.

As shown in Figure 2, the UV-visible spectra show that the absorption behaviors of the prepared films are different from each other depending on their composition. Film 4 (PVA only) shows an intense absorption peak around 200 nm originating from intrinsic electronic transitions of polymer structure. The absorption peak for Film a (PVA+ZnO) was displaced to 210 nm, demonstrating that the electronic environment of the polymer changed due to the nanoparticle intercalation with the PVA film. In comparison, the absorbance peak of Film 2 (PVA+Alhagi) showed a relatively much higher blue shift than that for the pure analog of the PVA film and moved toward lower wavelengths of about 260 nm. The possible explanation would be due to phenolic and flavonoid materials located in *Alhagi maurorum* since these sorts of aromatic

compounds typically catch light at this UV range. Film 3 (ZnO/Alhagi/PVA) displayed a red shift and the highest absorption at 280 nm. The upward trend in the wavelengths from fig 2, d to c indicates improved molecular interaction within the composite structure.

Four transform infrared (FTIR) for synthesized film: FTIR spectroscopy (Figure 3) was used to investigate the chemical functional groups and molecular interactions present in the synthesized films. The pure PVA spectrum (Figure 3,4) showed characteristic peaks corresponding to the polymer backbone like O-H stretching and C-H vibrations. New absorption bands were formed, and the intensity of some peaks changed by adding ZnO nanoparticles (Figure 3,1) and Alhagi extract (Figure 3,2). Interestingly, the combined spectrum for the ZnO/PVA/Alhagi nanocomposite (Figure 3,3), as illustrated in Figure 3.3, indicates a plausible chemical interaction between the plant product and ZnO, suggesting an effective bonding of both by cooperative entrapment within the PVA matrix. FTIR spectra of the synthesized metal films: (Figure 3,1) ZnO/PVA film showing bands typical of PVA and a new peak at 701 cm^{-1} due to ZnO stretching, confirming the presence of zinc oxide nanoparticles; (Figure 3,2) Alhagi/PVA films also show peaks at 1600 cm^{-1} (C=C aromatic stretching), suggesting their content of phytochemicals such as flavonoids and phenolics from the *Alhagi maurorum* extract. (Figure 3,3) ZnO/Alhagi/PVA composite film showing merged characteristics of XZ and Alhagi extract by minimal shifts in O-H (3436 → 3435 cm^{-1}) and C=C (1637 → 1634 cm^{-1}) peaks due to intermolecular interactions along with hydrogen bonding within the matrix. (Figure 3 ,4) Pure PVA film exhibiting a broad O-H stretching band at 3436 cm^{-1}, C-H stretching at 2079 cm^{-1}, and C-O stretching near 1095 cm^{-1} (Figure 3,1). The FTIR measurement of the ZnO/PVA combination films revealed characteristic peaks, indicating the successful incorporation of both components. The stretching vibrations of the C-O bonds inside the PVA backbone were responsible for the peaks seen at 1066 cm^{-1} as well as 1100 cm^{-1}. Furthermore, the PVA polymer chain's C-H bending vibrations correlated with peaks at 1200 and 1300 cm^{-1}. A strong peak at 701 cm confirms the presence of ZnO nanoparticles inside the composite matrix, likely due to the Zn-O bending vibration (Figure 3.2). The FTIR examination of the PVA/Alhagi hybrid films revealed characteristic peaks, indicating the good integration of both components. The stretching vibrations of the C-O bonds in the PVA backbone were responsible for the noticeable peak at 1070 cm^{-1} . Moreover, the PVA polymer chain's C-H bending vibrations correlated with peaks at 1260, 1300, and particularly 1400 cm. O-H stretching vibrations from the hydroxyl groups in both PVA and the Alhagi extract probably caused the large peak at 3300 cm^{-1}. Another possible indication of carbonyl groups (C=O) in the Alhagi extract, perhaps from chemicals like flavonoids, is the existence of a peak at 1600 cm^{-1} (Figure 3.3). The distinctive peaks at 400 cm^{-1} seen in the FTIR study of the ZnO/PVA/Alhagi hybrid films are most likely caused by the Zn-O vibrations that stretch of ZnO. The C-O stretching vibrations within the PVA backbone were confirmed by the peaks at 1000-1100 cm^{-1}.

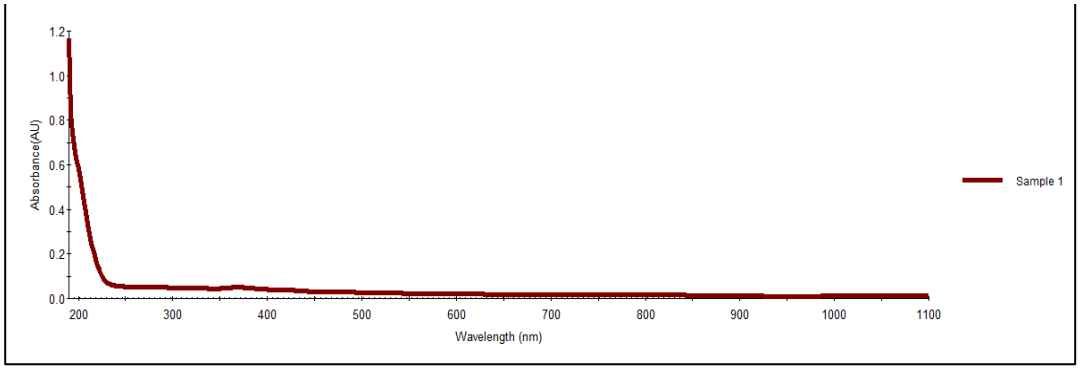

a

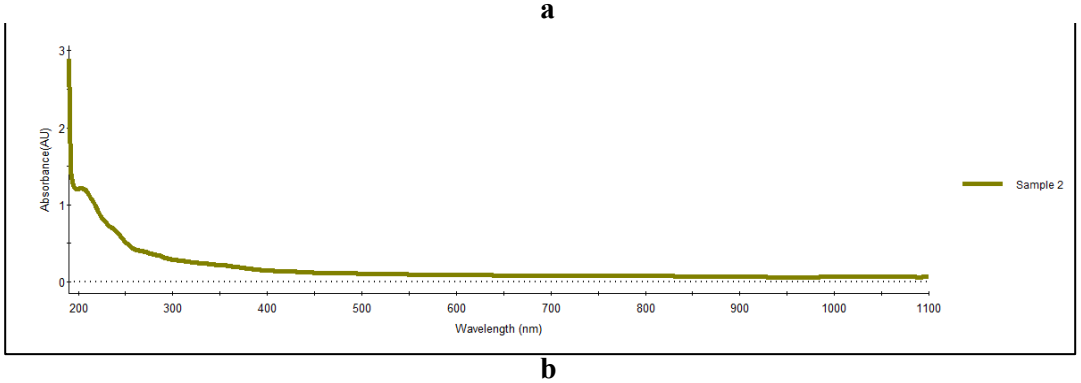

b

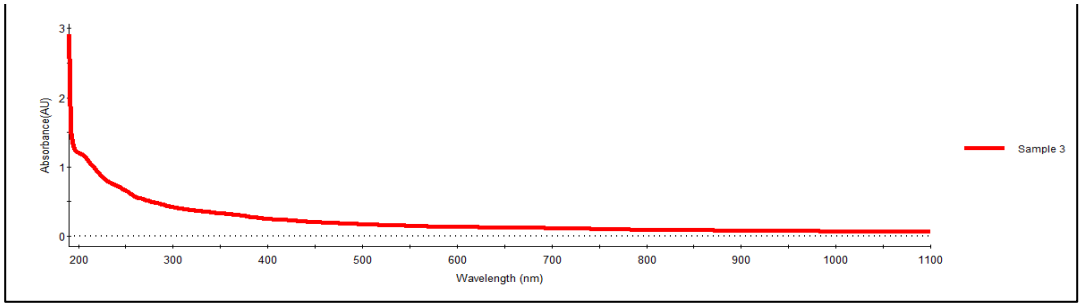

c

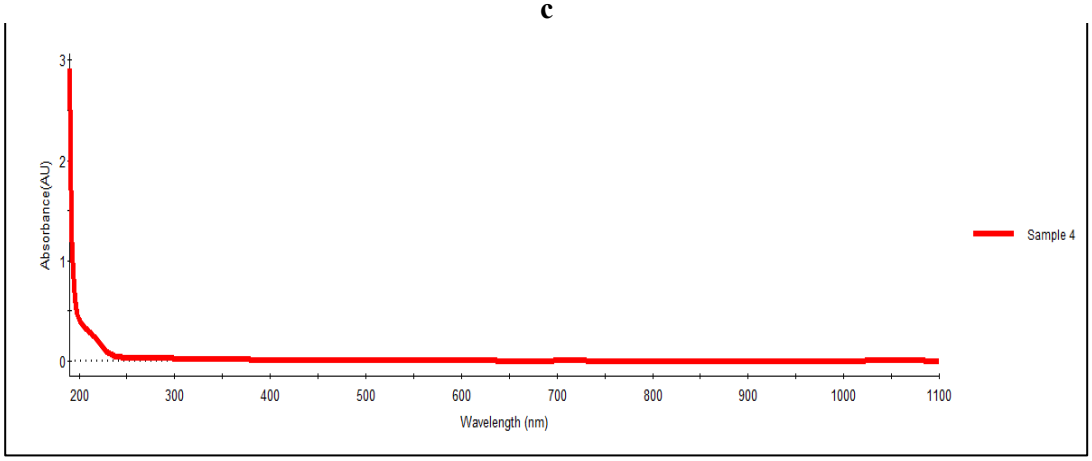

d

Figure 2. Illustrates the UV absorbance values for the following: a) ZnO and PVA, b) ZnO and Alhagi, c) ZnO nanoparticles with PVA and Alhagi maurorum, and d) PVA alone.The comparison illustrates the successful integration of the nanoparticles and plant extract into the polymer matrix

Furthermore, there were peaks in the 1300-1400 cm^{-1} range with 2900-3000 cm^{-1} bands, which may correspond to C-H stretching and bending vibrations in PVA and perhaps organic components in the Alhagi extract, respectively. These results proved that the Alhagi extract, ZnO, and PVA were all properly mixed into the matrix of the composite film. (Figure 3.4) FTIR examination of the PVA films revealed distinct peaks that point to the structure of the polymer. Peaks at 1070 cm^{-1} as well as 1100 cm^{-1} were determined to be caused by C-O stretching vibrations in the PVA backbone. Peaks at 1140 cm and 1180 cm further confirmed the existence of PVA, most likely due to stretching C-O-C vibrations. There were also peaks at 1270 cm^{-1} and 1360 cm^{-1}, which show that the C-H stretching vibration is happening in the PVA polymer chain. The wide peak located at 3400 cm confirmed the presence of O-H stretching vibrations emanating from the hydroxyl groups in PVA (Figure 3, 4).

Scanning electron microscope of the film complex: The morphology of nanoparticle-embedded films was selectively examined by FESEM analysis. This characterization is only for the ZnO/PVA and ZnO/PVA/*Alhagi maurorum* nanocomposite films due to their metallic nano-fillers, which are important for our study. For each sample, two different magnifications were used to obtain a clear structural overview. The micrographs at high magnification (500 nm) were used to detail the fine structures of synthesized nanoparticles and demonstrate spherical shape and size distribution. While, in the 500x magnification images, 100 micrometers were registered to analyze the surface topography and dispersion degree. The uniform and homogeneous distribution of components in the polymeric matrix was confirmed by examining these images, which show that both the plant extract and nanoparticles are successfully embedded into the melt blend (Figure 4 a, b and d). The ZnONPs/PVA film showed that spherical ZnO nanoparticles are distributed in the polymer matrix with a size between 11 and 55 nm. Some parts of the area showed slight aggregation. The ZnONPs/Alhagi/PVA film (Figure 4c) has a narrower size distribution of 20-44 nm, suggesting a better homogeneous spread in the matrix. These structures looked lamellar-like and presented as a dense, compact matrix with no evidence of particle formation. Micrometer thicknesses of the active film (around 1-2 μm) were measured.

Scanning electron microscope of the film complex: Figure 4 (a and b) shows the FESEM fracture surface of the PVA and biocomposite films. The homogenous polymer structure is connected with propagation. After adding plant extract as well as ZnO nanoparticles, the surface becomes rougher.

X-Ray diffraction analysis (XRD): X-ray Diffraction (XRD) was used to characterize the crystalline phases and structural orientation of ZnO/Alhagi/Alhagi film. The obtained diffraction pattern (Fig 5) showed several well-defined peaks at 2θ° values of 43.054°, 50.138°, 73.627°, 89.278°, 94.426°, 115.863°, and 134.871°.These particular reflections relate to the crystallographic assignment as follows: 34° (002): Main characteristic peak of hexagonal Wurtzite ZnO structure; 50°, 73°, and 89°: secondary peaks corresponding to the (102), (110), and (103) planes of ZnO, respectively; 94°, 115°, and 134°: High-angle reflections for (200), (112), and (201) Miller indices (hkl), which provide more evidence of the high crystallinity of the nanoparticles incorporated into the polymer matrix (Figure 5) (Table 7).

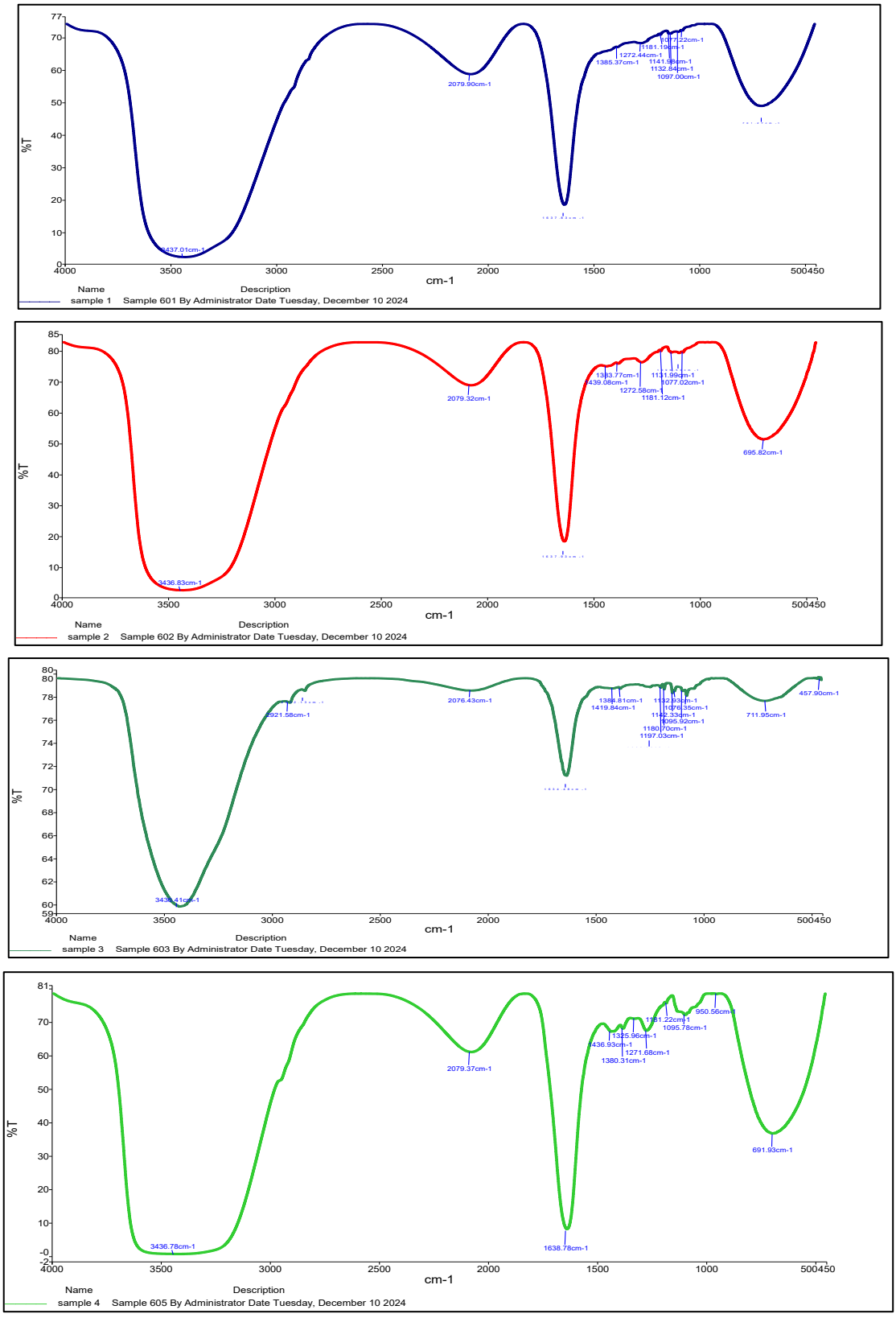

Figure 3. Revealed the results of FTIR for four samples: 1 refers to ZnO and PVA, 2 to Alhagi-PVA extract, 3 to the ZnO/PVA/Alhagi combination, and 4 to PVA alone

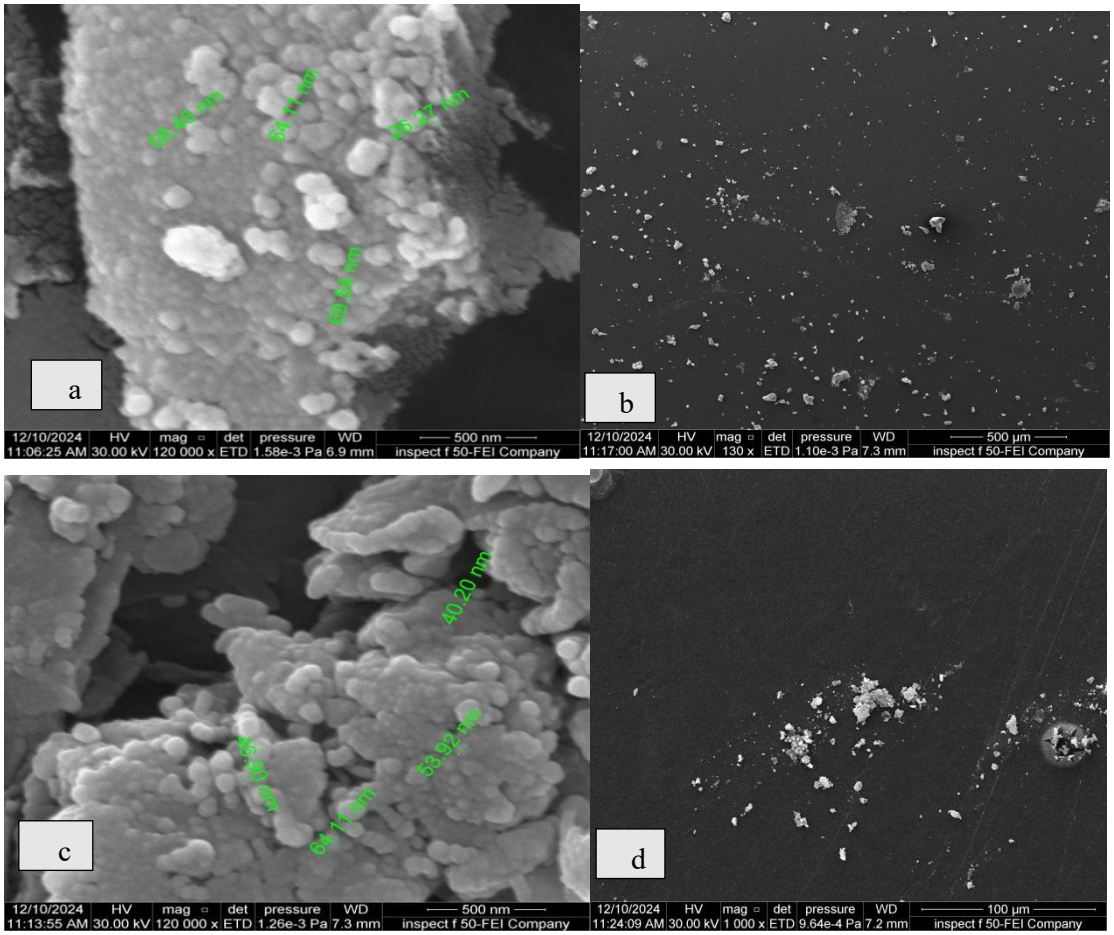

Figure 4. a and b: SEM of a refers to PVA+ZnONPs at 500 nm and 500 micrometer, c and d: refers to ZnONPs /Alhagi /PVA at 500 nm and 100 micrometers

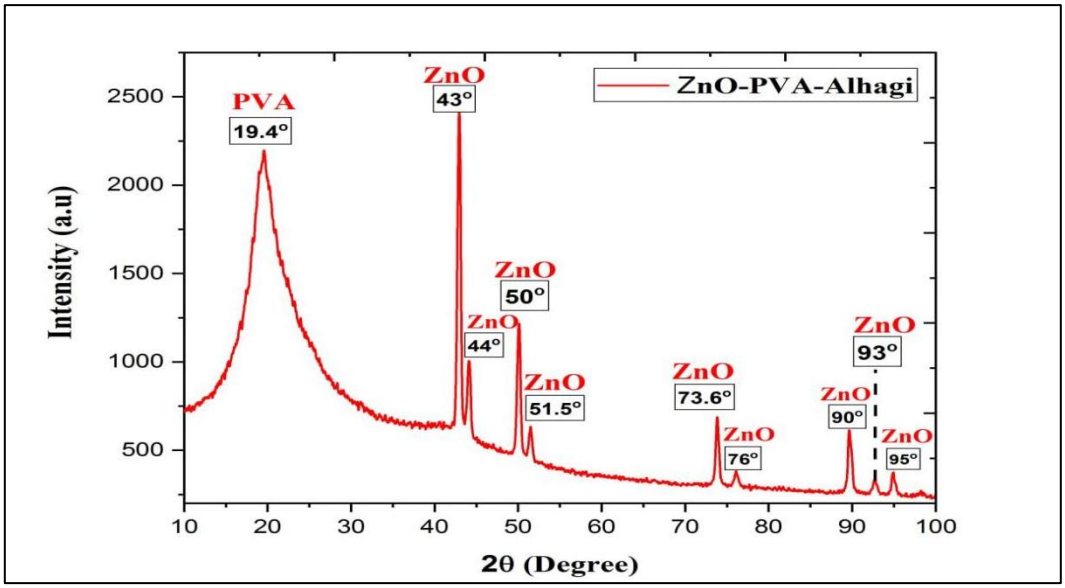

Figure 5. XRD patterns of ZnO/Alhagi/PVA *maurorum* composite film

The wide peak at $2\theta \approx 19.68°$ is associated with the semi-crystalline structure of the PVA polymer matrix, while the sharp reflections (asterisks) can be ascribed to the hexagonal wurtzite structure for integrated ZnO nanoparticles.

Table 4. The XRD peaks and Miller indices (hkl) for ZnO nanoparticles

θ2	hkl	Material
19.4	amorphous	PVA
43	(101)	ZnO
44	(102)	ZnO
50	(110)	ZnO
51.5	(103)	ZnO
73.6	(202)	ZnO
76	(004)	ZnO
90	(203)	ZnO
93	(210)	ZnO
95	(211)	ZnO

Note: Using the Scherer equation on the most intense peak (101), it was found that the average crystallite size was around 20 nm. The sharp nature of the peaks indicates a high crystallinity of the synthesized ZnO.

Antioxidant results: Maximum antioxidant activity for the third combination of ZnO/Alhagi/PVA film was observed in a concentration-dependent manner. The antiviral effect produced in vivo exhibited antioxidant potential at a concentration of 1 mg/mL (83.16% inhibition) compared to the standard ascorbic acid 96.24%. From the curve of inhibition values plotted on a semi-logarithmic scale, the estimated IC_{50} that inhibited 50% DPPH radicals in this context was found to be 0.25 mg/mL (Figure 6). The ability of the ZnO/Alhagi/PVA nanocomposite to eliminate free radicals was measured using the DPPH assay. The lowest dose (0.125 mg/mL) of the test compound exhibited 45.85% inhibition in growth, and the highest dose (1.0 mg/mL) significantly exhibited up to 83.16% inhibition in growth, respectively. Our composite was very competitive with respect to the ascorbic acid tested. This means it is a strong antioxidant, as the IC_{50} (the amount required to block half the radicals) was only 0.18 mg/mL. It was successfully achieved through a combination of zinc oxide nanoparticles [ZnO NPs], introduced in a PVA (polyvinyl alcohol) matrix, and Alhagi plant extract. This synergism increases antioxidant capacity since it conforms to new and innovative utilization within cosmetic formulations and wound plasters, particularly in skin protection in cosmetics or healing power between wounds (Figure 6).

AST Profile of *P. aeruginosa:* All isolates are multidrug-resistant (MDR), with nearly all showing extensive β-lactam and fluoroquinolone resistance, and only amikacin retaining activity. The high resistance was recorded for ampicillin 90%, while 50% and 35% of the isolates were resistant to carbapenems (e.g., meropenem, imipenem) supports possible MBL gene carriage, such as bla IMP (Figure 7). All isolates are multidrug-resistant (MDR), with nearly all showing extensive β-lactam and fluoroquinolone resistance, and only amikacin retaining activity.

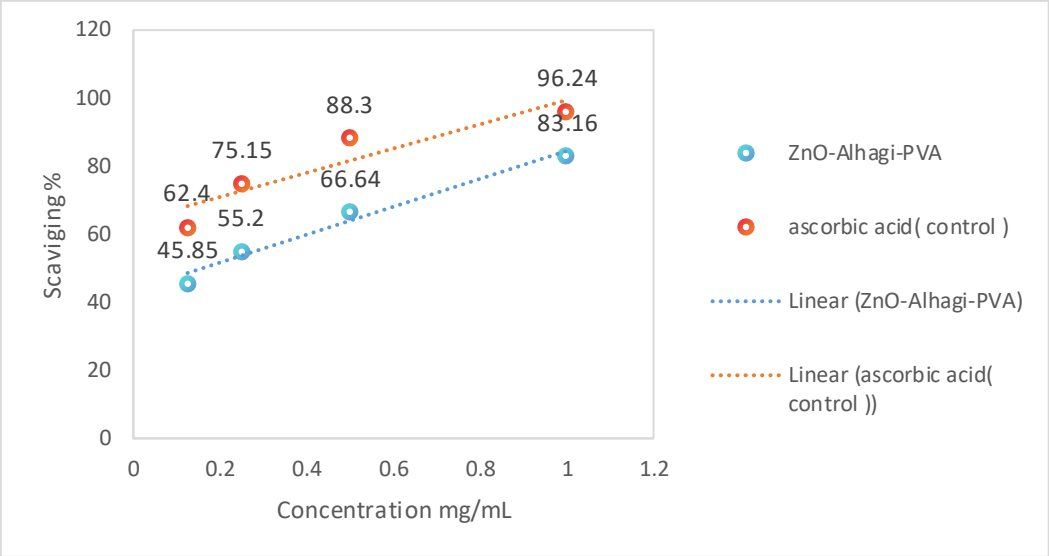

Figure 6. DPPH free radical scavenging activity of the ZnO/ Alhagi /PVA nanocomposite compared to ascorbic acid (standard antioxidant)

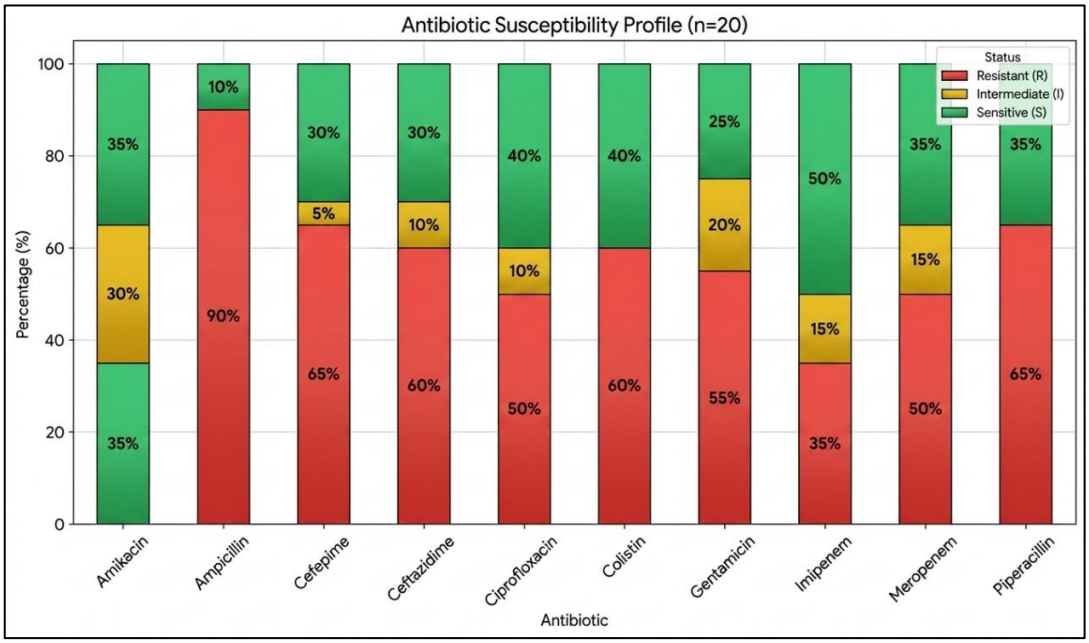

Figure 7. AST profiles of twenty *p aeroginosa* isolates

Antimicrobial film: Prepared films were evaluated using the Mueller-Hinton agar diffusion method against *Pseudomonas aeruginosa* that was isolated from burn infections and characterized as multidrug-resistant (MDR). The following film formulations were evaluated in total: (a) PVA/ZnO nanoparticles (ZnO NPs), (b) PVA with plant extract, (c) PVA/ZnO NPs with plant extract, and (d) control PVA. This clearly inhibited the growth of bacteria under and next to active composite films. In particular, ZnO NPs/plant extract /PVA film demonstrated the highest antibacterial activity with respect to this assessment, as no visible growth was observed in the contact zone. Other films with either ZnO NPs or plant extract alone developed significant

inhibition too, compared to the minimal or no antibacterial activity of PVA control. Notably, the tested strain was MDR and isolated from burn wounds (which typically are difficult to treat) so that its suppression is indicative of the potential usefulness of developed composite films as innovative antimicrobial materials in the management of resistant *P. aeruginosa* infections either as sole or adjuvant localized therapies (Figure 8).

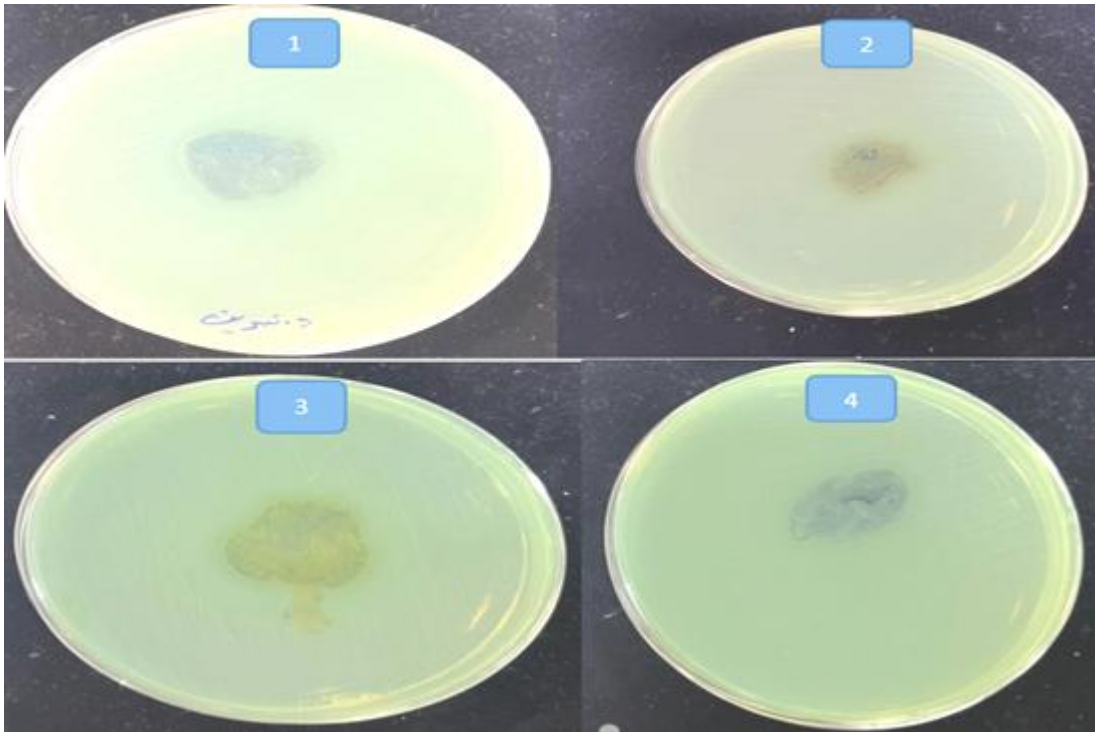

Figure 8. The antibacterial activity of the prepared films was evaluated on Mueller-Hinton agar using the agar diffusion method: (1) ZnO-PVA film; (2) Alhagi-PVA film; (3) ZnO-Alhagi-PVA ternary composite film; and (4) PVA-only film (control)

Antibacterial activity studies of synthesized films were carried out using the disc diffusion method on Mueller-Hinton agar. The ZnO/Alhagi/ PVA composite film showed an efficient inhibition, although it was limited to just below the film area, where there was no growth of bacteria directly under the composite (Figure 8,3). The localized nature of such activity suggests successful embedding of the antimicrobial agents in the polymer matrix, where they are effectively working through direct contact. ZnO-PVA and Alhagi-PVA films had high activity but moderate (68%) and low influence (16%), respectively, while PVA showed no inhibition (Figure 8 1,2,4). The pronounced improvement in antibacterial function post-impregnation of ZnO nanoparticles and plant extracts indicates a synergistic role (Figure 8,3). This contact killing mechanism is especially important for use in the context of wound dressing, where a sterile interface can be obtained at the wound bed and uncontrolled leaching of nanoparticles into surrounding tissues is avoided.

Genetic technique: All twenty isolates tested positive for the *blaTEM* and *blaIMP* antibiotic resistance genes, indicating that they are multidrug-resistant (MDR). The antibiotic susceptibility test (AST) using the VITEK® 2 system showed that all tested antibiotics were highly resisted, with some differences in how they responded to imipenem, where some were resistant and others

had intermediate sensitivity. On the other hand, molecular analyses showed that all isolates carry the studied resistant genes, indicating the virulence of these strains and their spread in the hospital environment. (Figures 9 and 10). The 20 *Pseudomonas aeruginosa* isolates from burn infections in Babylon, Iraq, all carry both *blaTEM* and *blaIMP* genes, indicating widespread multi-drug resistance. This phenomenon is a result of interconnected socio-economic, environmental, and healthcare factors unique to the Iraqi context.

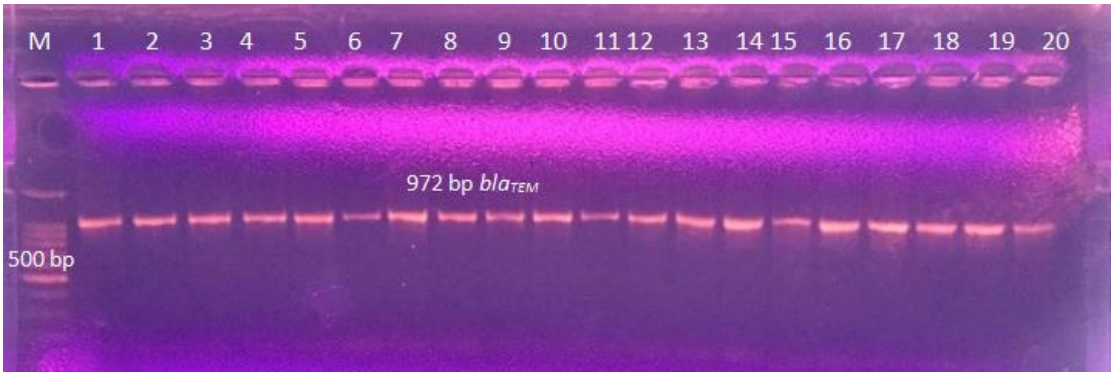

Figure 9. Agarose Electrophoresis of *blaTEM* Amplicon 972 bp, *P. aeruginosa* Isolated from Iraqi Patient (1.5% Agarose at 75 Volts for 45 min) Line M: DNA ladder (100 bp); Lines 1-20: positive results of amplification. Line M: marker

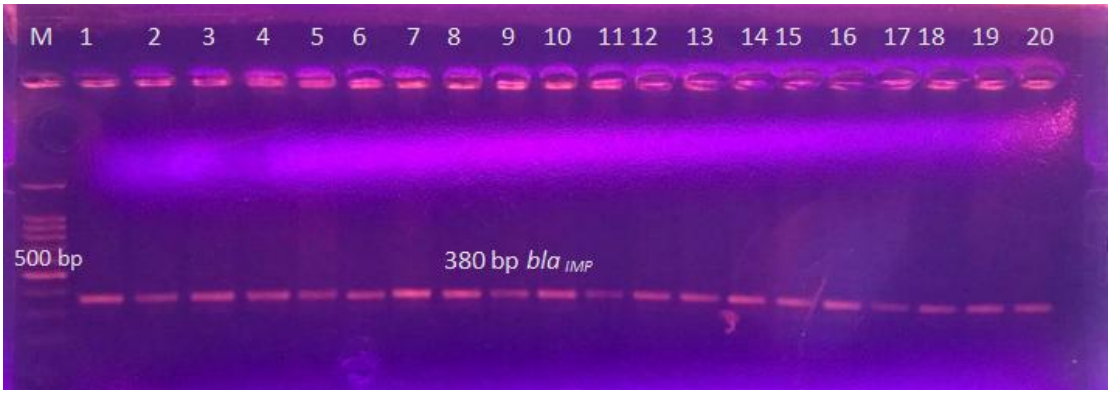

Figure 10. Agarose Electrophoresis of blimp Amplicon 380 bp among *P. aeruginosa* Isolated from Iraqi Patients (1.5% Agarose at 75 Volts for 45 min): Lines 1-20: positive results of amplification. Line M represents the marker.

The 20 *Pseudomonas aeruginosa* isolates from burn infections in Babylon, Iraq, all carry both *blaTEM* and *blaIMP* genes, indicating widespread multi-drug resistance. This phenomenon is a result of interconnected socio-economic, environmental, and healthcare factors unique to the Iraqi context.

Phylogenetic analysis comparative of *blatem* gene sequence: Figure 11 and 12 depicts the nucleotides distance phylogenetic tree of 13 *blaTEM* gene sequences originating from Pseudomonas aeruginosa, two were selected isolates recovered from burn infection in Iraq. The comparison was conducted on the base of pairwise genetic distances calculated from partial nucleotide sequences and presented in the form of a hierarchical clustering dendrogram and a

heatmap matrix. The Iraqi isolates (1_PX396140. 1 and 2_PX396141. 1) were analysed and compared to reference strains acquired from several regions of the globe, assessing their evolutionary relationships and genetic similarity. The color scale indicates the genetic distance values, with close genetic relationships and high sequence similarity among the studied taxa (0.00-0.01).

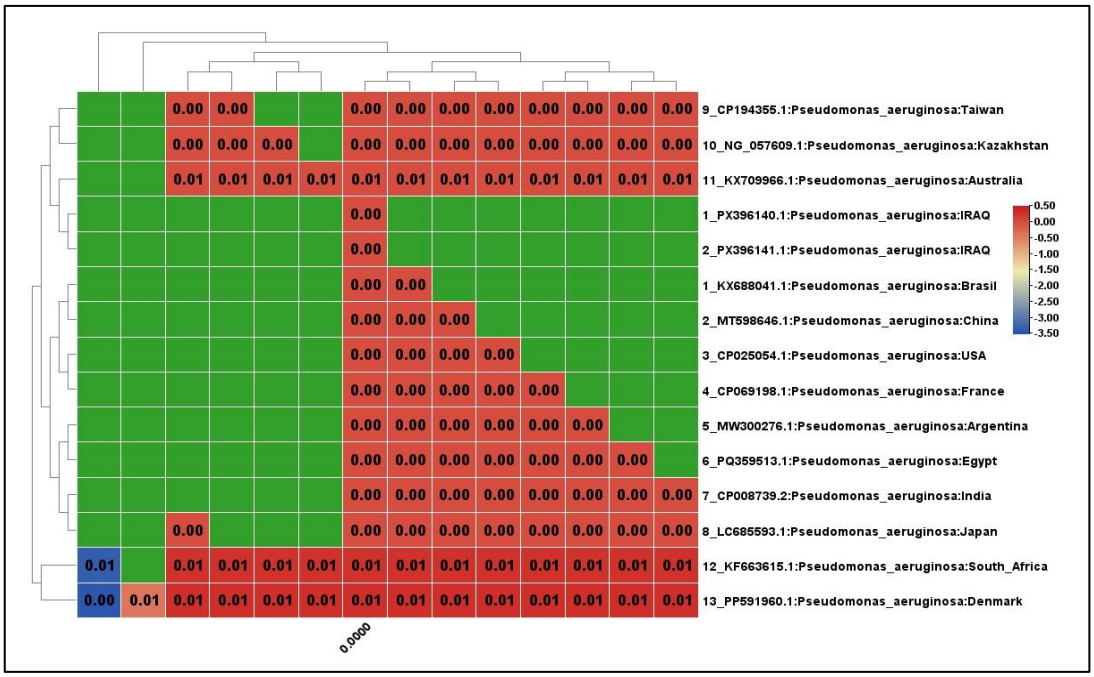

Figure 11. Similarity matrix of the degree of genetic relatedness among the studied taxa

Phylogenetic analysis indicated that Iraqi burn isolates were closely related to those from Brazil, China, USA, France, Argentina, Egypt, India and Japan (with 0.00 genetic distance). This suggests full or near-full sequence homology of the *blaTEM* gene region examined. In contrast, isolates from Australia, South Africa and Denmark differed by only 0.01 in identity. These findings by indicating such a high global identity between strains might also explain that *blaTEM* gene is highly conserved and will corroborate with the concept of international spread by horizontal transfer of genes (Figures 11 and 12).

DFT calculations: The electronic properties of the PVA-linoleic acid-ZnO complex were examined through frontier molecular orbital (FMO) calculations. The HOMO, LUMO, and HOMO-LUMO energy gap values are presented in Table 6. The results show that both the HOMO and LUMO energies are identical (-0.148523 eV), leading to an energy gap of 0 eV. This HOMO-LUMO gap suggests high electronic reactivity and low stability, as a narrower gap indicates that electrons can be excited from HOMO to LUMO with minimal energy input (Table 5). From a chemical reactivity perspective, the small gap implies that the PVA-linoleic acid-ZnO complex may readily participate in charge transfer interactions with biological targets, which could enhance its binding ability. However, the identical HOMO and LUMO values also suggest a

limitation in orbital differentiation, which might reduce selectivity in electronic transitions compared to systems with larger gaps (Figure 13).

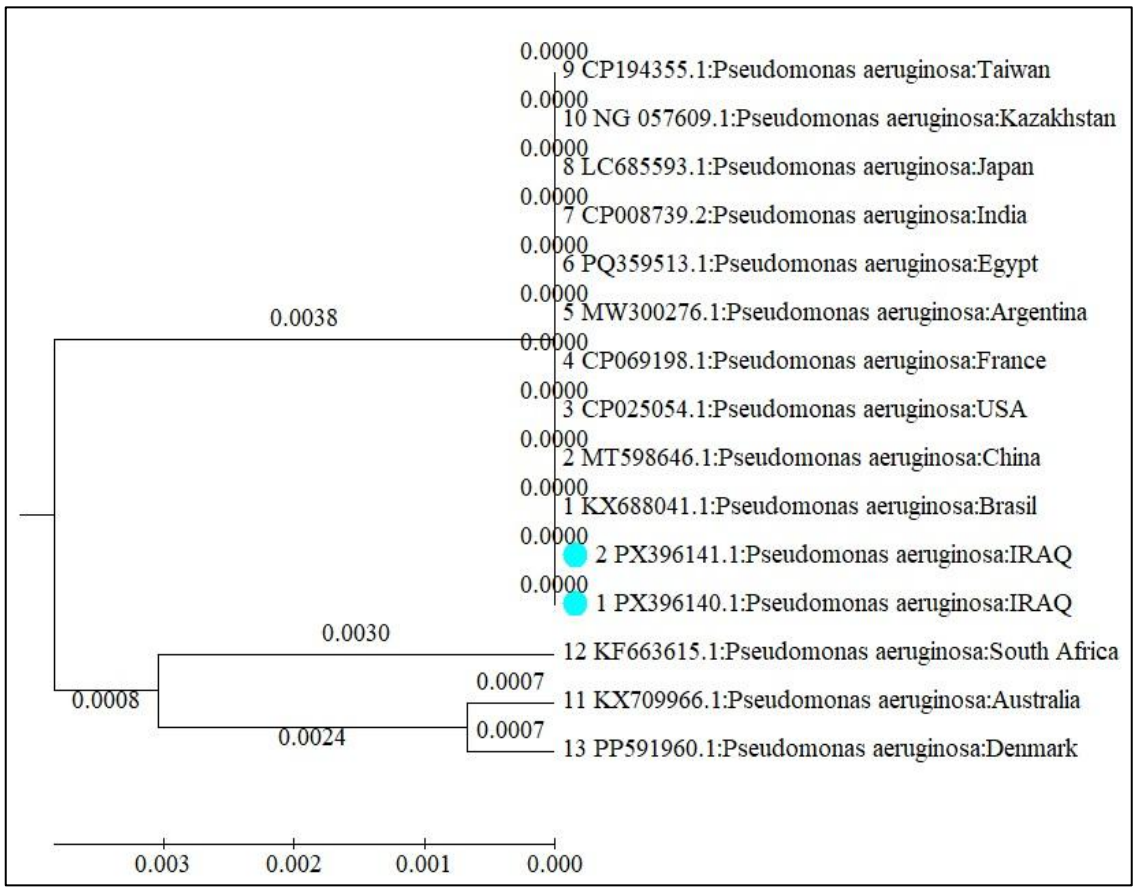

Figure 12. Evolutionary relationships of taxa

Table 6. HOMO, LUMO, and HOMO-LUMO gaps

Complex	HOMO	LUMO	HOMO-LUMO gap
PVA-Linoleic acid-ZnO	-0.148523	-0.148523	0

Molecular docking: The molecular docking is conducted to examine the binding affinities and molecular interactions of PVA-linoleic acid-ZnO with protein neuraminidase (4b7q). The molecular docking results of linoleic acid, polyvinyl alcohol (PVA), and zinc oxide (ZnO) nanostructures with the 4b7q protein are summarized in Table 6. The binding affinity, inhibition constant (Ki), RMSD values, and intermolecular energies were analyzed to evaluate the interaction strength and stability of the ligand-protein complexes. The docking study revealed that ZnO exhibited the strongest binding affinity with the 4b7q protein (Table 7), recording a binding energy of -7.29 kcal/mol and the lowest inhibition constant (4.55 μM). The relatively low RMSD value (2.421 Å) indicates a stable docking pose, supporting the reliability of ZnO's binding orientation. The final intermolecular energy of -7.88 kcal/mol suggests that van der Waals,

hydrogen bonding, and desolvation forces contributed favorably to the interaction. In contrast, linoleic acid showed moderate binding affinity (-4.45 kcal/mol) with a high inhibition constant (543.15 µM), reflecting weak inhibitory potential. Although the intermolecular energy was relatively favorable (-8.93 kcal/mol), the high RMSD (4.283 Å) indicates an unstable or less reliable docking conformation (Table 7). PVA displayed the weakest interaction with 4b7q, yielding the lowest binding energy (-1.22 kcal/mol) and a Ki of 127.71 µM. The higher RMSD (4.151 Å) further reflects a poor docking pose. This weak binding may be attributed to the limited chemical functionality of PVA for forming stable interactions with the protein's active site (Table 7).

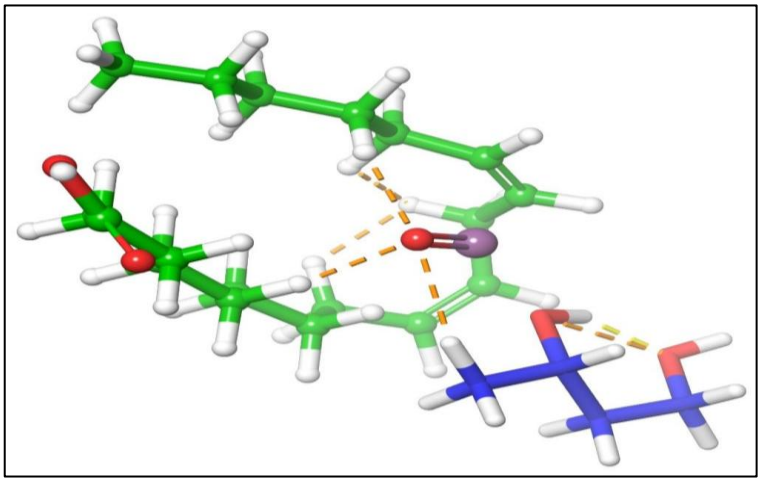

Figure 13. The molecular interaction of ZnO-linoleic acid-PVA after quantum computations

Table 7. The molecular docking results

Compound	Estimated Free Energy of Binding (kcal/mol)	RMSD (A)	Estimated Inhibition Constant, Ki (uM (nanomolar)	Final Intermolecular Energy = -9.23 kcal/mol USER vdW + Hbond + desolv Energy (kcal/mol)
		4b7q		
Linoleic acid	-4.45	4.283	543.15	-8.93
PVA	-1.22	4.151	127.71	-5.10
ZnO	-7.29	2.421	4.55	-7.88

Overall, these results suggest that the ZnO nanostructure has the highest binding potential toward the 4b7q protein compared to linoleic acid and PVA. The strong binding affinity and low inhibition constant of ZnO highlight its potential role as a stable binder or inhibitor, whereas linoleic acid and PVA are less effective.

Discussion

Unwavering dedication to the search for sustainable and natural therapeutics beyond that of traditional antomicrobial interventions is what forms the basis of scientific innovation in modern wound healing. This work results in the first ever combination of Alhagi extract, an Iraqi drought-tolerant plant, with ZnO NPs inside a biocompatible PVA polymer matrix. By exploiting this non-

toxic medical-grade scaffold to prevent the growth of antibiotic-resistant *Pseudomonas aeruginosa* in burn wounds, the current study provides a new clinically applicable tool for Iraqi patients as bioactive dressings or a topical cream. In addition to the empirical evidence, we believe that nature represents a rich source of chemically diverse bioactive compounds that can be exploited for biomedical applications. To identify the specific bioactive constituents responsible for this therapeutic breakthrough, GC-MS analysis was conducted, revealing a complex profile of 12 phytochemicals. Among these, Linoleic Acid was strategically selected as the lead ligand for Molecular Docking simulations. GC-MS analysis of the methanolic extract from the aerial parts of *Alhagi maurorum* revealed twelve phytochemicals (Table 3, Figure 1.a; b). Key molecules such as 1-(2-Phenyl-1,3,2-dioxaborolan-4-yl)-1,2-ethanediol, phthalic acid, 7,8-diazabicyclo[4.2.0]octane, 1-methyl-, 7,8-dioxide, 9,12-octadecadienoic acid (linoleic acid), and 2-amino-2-oxoethyl acetate were classified as phenolic, boronate, or fatty-acid-derived compounds. These structural classes are known for their antioxidant and antimicrobial activities; for example, linoleic acid and aromatic acids disrupt bacterial membranes and inhibit microbial growth. Notably, boronate-containing molecules, like the detected dioxaborolane derivative, have garnered attention as enzyme-inhibiting antibacterials. In contrast, detected hydrocarbons and silane derivatives (e.g., toluene, trimethyl(n-pentyl)silane, 1-butyne) were classified as biologically inert under typical assay conditions. Overall, the predominance of phenolic and fatty acid esters in the extract provides a chemical basis for the observed DPPH radical scavenging and antibacterial activity of the PVA-Alhagi composite film (Figure 6). These findings align with prior research demonstrating that phenolic-rich Alhagi extracts possess significant free radical scavenging and antimicrobial efficacy. Notably, boronate-containing compounds, such as the identified dioxaborolane derivative, have received interest as enzyme-inhibiting antibacterials. Under standard laboratory settings, identified hydrocarbons and silane derivatives (such as toluene, trimethyl(n-pentyl)silane, and 1-butyne) were classed as biologically inert. Its high phenolic and fatty acid ester content supports the PVA-Alhagi composite film's antibacterial and antioxidant properties. Previous research suggests that phenolic-rich Alhagi extracts have antibacterial and free radical scavenging properties. The PVA-Alhagi composite film's antioxidant and antibacterial properties are attributed to its high phenolic and fatty acid ester content, which align with previous research suggesting strong free radical scavenging and antibacterial properties (Abdulbary, 2019; Mostafa & Essawy, 2019). A GC-MS analysis of the extract of the plant *Alhagi maurorum* (Alkool) from the Hilla region in central Iraq determined a putatively identified compound (1-(2-Phenyl-1,3,2-dioxaborolan-4-yl)-1,2-ethanediol) based on GC-MS library matching (Table 3). This compound is one of the cyclic compounds that contain the element boron, an uncommon chemical class found in plant extracts, particularly in wild plants. When searching for *Alhagi maurorum* components, it was discovered that this molecule is not recorded in plant chemistry databases such as PubChem. The presence of this compound in this specific plant from the Iraqi environment is thought to be related to local environmental factors such as soil type, salinity, high temperatures, and the nature of the irrigation water, all of which have been shown to directly affect the production of secondary compounds in plants, including those with unconventional biological activity. Previous researches (Muhammad et al.,

2024; Eftekhari et al., 2025) have confirmed that environmental stresses like salinity and drought cause changes in gene expression within plants, resulting in the emergence of new compounds with unique chemical structures that are not found in other plant environments (Figure 1 a and b).

Optical and structural characterization of the nanocomposite film: The successful incorporation of ZnO nanoparticles into the Alhagi/PVA matrix was achieved through UV-Vis spectroscopy, that showed the absorbance red shifted progressively with increasing complexity of the film composition. An absorption peak of PVA has been observed at 200 nm in Film 4 (PVA only), which corresponds to the optical property of pure PVA matrices (Brzęk & Sterzyński, 2020). Notably, incorporation of ZnO nanoparticles (Film 1: PVA+ZnO) shifted the absorption to higher energy at 212 nm due to modification of the polymer's electronic structure upon interaction with nanoparticles and band gap (Wen et al., 2022). The inclusion of the phytocomponent-rich *Alhagi maurorum* extract in Film 2 (PVA+Alhagi) is also shown to induce a more obvious and marked shift towards 260 nm due to some classes of UV-absorbing phenolic and aromatic phytochemical groups (Yue et al., 2023). The highest absorption was observed at 280 nm in Film 3 (ZnO+Alhagi+PVA), suggesting possible synergetic interactions between ZnO nanoparticles and bioactive components present within the PVA matrix. It is essential to note that the gradual bathochromic shift from Film 4 to Film 3 strongly affirms successful nano-integration and more intermolecular interaction among varying molecules as well, and its UV-absorbing criterion has been enhanced, which can correlate with its dramatic biomedical utility (Figure 2, a, b, c, d). To further investigate the chemical interactions and molecular bonding between the PVA hydroxyl groups, the Alhagi phytochemicals, and the ZnO surface, FTIR analysis was performed. The results of A pure PVA film show the typical broad O-H stretching band between 3300 and 3400 cm^{-1} corresponding to the hydrogen bonding in the polymeric matrix. Frequencies between 1080 and 1140 cm^{-1} correspond to C-O stretching vibrations, and peaks yielded by bending vibrations of C-H are shown in the region of 1320-1420 cm^{-1} (Abdelrazek et al., 2019). These results are in good agreement with recent spectroscopic work on PVA-based films, supporting its semicrystalline structure and hydroxyl-rich backbone (Sabr et al., 2024). The peak region (400-600 cm^{-1}) represents the lifetime band of Zn-O stretching vibrations, confirming that ZnO nanoparticles are incorporated in the PVA polymer matrix to form the composite film. Overall slight broadening of the O-H band indicates intermolecular interactions between ZnO NPs and PVA hydroxyl groups. This spectral behavior is akin to the previous ZnO/PVA nanocomposites consisting of interfacial interaction and hydrogen bonding; consequently, this led to more structural compatibility (Sabr et al., 2024). In the PVA-Alhagi hybrid film, broad O-H stretching band peak enhancement and peaks at ~1600 cm^{-1} indicate phenolic and carbonyl groups from bioactive phytochemicals in the plant extract. We characterize these bands, which are typically connected with flavonoids and polyphenolic constituents. Several FTIR studies on PVA films containing plant extracts have described similar spectra, indicating successful mixing mainly through hydrogen bonding and not covalent modification. Characteristic bands of each component are visible in the ternary ZnO-PVA-Alhagi composite, such as those related to Zn-O vibrations (≈400-500 cm^{-1}), C-O stretching (1000-1100 cm^{-1}), and O-H elongation (~3300 cm^{-1}). The presence of these peaks along with the one-of-a-kind disappearance indicates improvement

in the dispersion and mutual physical interaction among ZnO nanoparticles, PVA chains, and phytoconstituents. Similar hybrid systems observed in recent literature of such interactions exhibited mechanical stability and enhancement of antibacterial effects while retaining the integrity of the chemical structure (Hussein et al., 2025). Generally, the FTIR results confirm the successful formation of composite films and also suggest that the interaction mechanism between bioextract and composite film is controlled primarily through hydrogen bonding and interfacial coordination, which agrees with other recent polymer-metal oxide-bioexcipient system studies (Figure 3). To visualize the internal architecture and surface topography of the optimized therapeutic platform, FESEM analysis was performed specifically on the ZnO/Alhagi /PVA nanocomposite film, as it exhibited the superior biological activity in preliminary screenings. Morphological observations of the films provide conclusive evidence for expedient blending of the ZnO NP into the PVA matrix. The minimal aggregation noted in the PVA/ZnONPs film can be attributed to the high energy surface and inherent tendency of ZnO nanoparticles to aggregate inside polymer systems (Ahmed et al., 2016; Xie et al., 2024). The better dispersion and narrower size distribution in the ZnONPs /Alhagi /PVA film indicate that phytochemical compounds present within the plant extract served as stabilizing and capping agents, preventing nanoparticle agglomeration while also improving compatibility with the PVA (Barbălată-Mândru et al., 2022). The banded lamellar morphology of pure PVA at 500 nm was due to the semi-crystalline nature of PVA resulting from intermolecular hydrogen bonding occurring during film formation (Abazari et al., 2025). The presence of ZnO increased the surface roughness, and that of the extract improved stabilization and dispersion of the nanostructures in the polymer matrix (Figure a, b, c, d). While, the FESEM micrographs visualized the spherical morphology and 20 nm size of the particles. XRD patterns were recorded to confirm the internal crystalline structure and to verify that the ZnO remained chemically stable within the PVA-Alhagi matrix.The extended PVA peak at 19.68 suggests a decrease in the crystallite nature of the polymer matrix. This structural change indicates that the molecules of *Alhagi maurorum* extract have effectively intercalated between PVA chains, hindering their orderly packing, a behavior that is in accordance with observations made by Abdelrazek et al. (2010). The presence of intense peaks in the range of 42˚ to 50˚ verifies the successful development of the ZnO crystalline phase inside of the composite. These peaks are consistent with the hexagonal wurtzite structure of ZnO. The stability of the film seems to be improved by interaction between the ZnO surface and functional groups of the extract. Such a crystalline profile of ZnO is crucial for the antibacterial activity of the film against Pseudomonas aeruginosa, since bacterial killing by ZnO is directly correlated with its crystalline structure that forms reactive oxygen species (ROS) (Vasile & Baican, 2021). The addition of ZnO nanoparticles to PVA introduces a crystalline hybrid structure with distinct diffraction peaks attributed to different ZnO phases. The slight shift and broadening of these peaks in the ZnO/Alhagi/PVA composite phase implied a change in lattice spacing and decreased crystallite size, indicating that there is strong interfacial interaction between the polymer matrix and inorganic nanoparticles; as in the case of ZnO/PVA composites, it has been shown that PVA addition affected peak intensity (Asadpour et al., 2022). Additionally, the appearance of a broader and less intense peak in the Alhagi/PVA film confirms that PVA was mainly in an amorphous state, whereas bioactive

constituents of the plant extract hindered polymer crystallization, which has been previously reported in different bio-nanocomposites where natural additives are able to prevent chain ordering (Premkumar, 2024). Such structural changes shifts in peaks, reduced intensity of the peaks, and peak broadening can imply that the plant extract causes a distortion of the lattice and also increases the dispersion of ZnO nanoparticles throughout the matrix, thus achieving different crystalline properties in the obtained composite films. Such changes can affect not only the mechanical but also the optical and functional properties, as documented in recent investigations of ZnO/PVA-based nanocomposites (Figure 5) (Table 4). Beyond its potent antibacterial performance, the multi-functional nature of the ZnO/Alhagi/PVA film was further evaluated through its antioxidant capacity. The results of the DPPH radical scavenging assay demonstrated a significant, dose-dependent antioxidant activity, with the hybrid film achieving a scavenging percentage of [66 %] at 0.5 mg/mL. The remarkable free radical scavenging activity was mainly ascribed to the existence of bioactive secondary metabolites, including flavonoids and phenolic compounds formed from *Alhagi maurorum* extract.A scavenging activity of 66% is observed, which indicates the hydrogen atom donating capacity of the composite film to deactivate DPPH free radicals. The incorporation of ZnO nanoparticles resulted in acting as electron transfer promoters at the interface of the film (Sirelkhatim et al., 2015). This antioxidant efficiency is important for biomedical applications due to its implication in the reduction of oxidative stress related to chronic bacterial infections (Figure 6). To establish the clinical significance of this study, the Antimicrobial Susceptibility Testing (AST) was performed on 20 *P. aeruginosa* isolates recovered from burn wound infections. The very high resistance rates in *Pseudomonas aeruginosa* isolates reflect the global dissemination of multidrug-resistant (MDR) strains, notably those containing extended-spectrum β-lactamase (ESBL), such as blaTEM, and metallo-β-lactamases (MBLs), e.g., blaIMP, conferring a broad spectrum of β-lactam resistance (Qin et al., 2022). The higher rates of carbapenem resistance (85%) may be related to MBL production, and aztreonam resistance may indicate the coexpression of other β-lactamases like ESBLs or AmpC enzymes (Shalmashi et al., 2022). Resistance to fluoroquinolone and aminoglycoside may be associated with efflux pump overexpression, QRDR mutation, and aminoglycoside-modifying enzymes (Castanheira et al., 2021). The semi-susceptibility to amikacin (15-20%) highlights its potential as a salvage treatment option (Saber et al., 2022). The detection of high-level colistin resistance because of chromosomal mutations in regulatory genes (pmrAB, phoPQ) or the acquisition of plasmid-mediated mcr genes (Singh et al., 2025). Collectively, the broad resistance profile indicates that multiple (different) determinants of resistance may coexist, which points to the importance of molecular surveillance and rigorous antimicrobial stewardship in clinical as well as agricultural settings (Radi & Al-Marzoqi, 2022). In stark contrast to these failing conventional antibiotics, the PVA-ZnO-Alhagi nanocomposite film demonstrated superior inhibitory action against the same 20 resistant isolates (Figure 7).

Antibacterial activity of ZnONPS/Alhagi/PVA films: Albeit both genes, bla_IMP and bla_TEM, were discovered to be upregulated among all 20 isolates, the ZnO/Alhagi/PVA nanocomposite film exhibited a powerful inhibitory effect through a contact-killing approach. This study explains that the localized biocidal property of the film conferred via synergism

between 20 nm ZnO and linoleic acid in this specific example has effectively outmaneuvered the range of enzymatic defenses that have inhibited conventional antibiotics.This observation suggests a contact-mediated killing mechanism rather than a passive diffusion process. This phenomenon is directly attributed to the strong intermolecular hydrogen bonding identified in the FTIR and Molecular Docking analyses, which effectively 'anchors' the 20 nm ZnO nanoparticles and the Alhagi bioactive compounds (such as Linoleic Acid) within the cross-linked PVA network (Figure 8). The high concentrations of Alhagi extract containing phytochemicals like flavonoids and phenolics as stabilizing and capping agents can significantly improve the antimicrobial properties of these nanocomposite systems (Al-Snafi, 2015). Antibacterial testing studies of *Alhagi maurorum* extracts alone reported different results, subject to extraction method and bacterial strain (Hussein et al., 2025), some confirming inhibition against Gram-negative and Gram-positive bacteria, suggesting its potential as a natural antimicrobial source when appropriately formulated. Meanwhile, the bioactive compound of Alhagi extract could probably interact with bacterial cell walls and other intracellular targets to produce a synergistic inhibition effect when combined with nanoscale ZnO.The improved dispersion of ZnO NPs in the presence of plant extract may also play a role in better antibacterial activity than binary PVA-ZnONPs films, as enhanced distribution of nanoparticles increases contact surface area with bacterial cells. The low level of antibacterial activity produced by the PVA matrix, in isolation, correlates with its nature as an inert polymer lacking intrinsic antimicrobial properties (Udayagiri et al., 2024). Overall, the results show the development of hybrid nanocomposite films containing natural plant extracts and metal oxide nanoparticles as potential antibacterial materials. This study revealed for the first time that using extracts from Alhagi maurorum, a native and underutilized plant in Iraq (and beyond), to produce advanced antimicrobial biomaterials would intensify antibacterial action in composite systems content with commercial antibiotics acting as therapeutic agents against difficult microorganisms (Figure 8).

Molecular genetic results: Genetic detection presents an unusual 100% prevalence of both resistance genes in the sample collection set. In all 20 isolates, class B beta-lactamase genes (blaIMP) were present; they are active against penicillins and cephalosporins , as well as class A beta-lactamase genes (blaTEM), indicating solid genetic machinery to neutralize the antibiotic. These findings correlate well with the MDR (multidrug-resistant) strains that were recovered from the burn wound infections and confirm these isolates as a serious clinical threat. In this study, both genes were identified in 100% (20/20) of isolates, indicating a considerable burden of resistance determinants. Researchers have now widely reported the dissemination of ESBL- and MBL-producing *P. aeruginosa* around the globe, particularly in high-risk hospital units such as burn wards (Shalmashi et al., 2022). Casual readers will be able to tell that the co-existence of ESBL and MBL genes in one isolate allows for an expanded resistance profile against penicillins, cephalosporins, and carbapenems, thus hindering the therapeutic approach (Bush & Bradford, 2020). These genes can coexist in the same isolate, conferring resistance to penicillins, cephalosporins, and carbapenems (Bush & Bradford, 2020), making therapeutic management extremely difficult. The findings underscore the contribution of molecular surveillance as well as

phenotypic testing to inform stewardship and infection prevention programs especially in health-care settings with high rates of resistance (Figures 9 and 10).

NCBI submission and phylogenetic analysis of Iraqi *blaTEM* sequences: Genetic data for two *blaTEM* gene sequences was successfully submitted to the NCBI GenBank database, and official accession numbers (PX396140.1 and PX396141.1) were obtained from clinical isolates of *Pseudomonas aeruginosa* collected through an extensive study in Iraq. GenBank, a publicly available nucleotide sequence repository and part of the International Nucleotide Sequence Database Collaboration (INSDC) (Benson et al., 2013), Unweighted Pair Group Method with Arithmetic Mean (UPGMA) phylogenetic analysis was performed. The Maximum Composite Likelihood (MCL) model, which estimates the number of nucleotide substitutions per site without assuming equal rates of substitution (Tamura et al., 2013), was used for calculating evolutionary distances. Evolutionary analysis was done using 15 nucleotide sequences, which include two newly deposited Iraqi *blaTEM* and reference sequences obtained from GenBank. Codon positions analyzed included the 1st, 2nd, 3rd, and non-coding regions. All missing outcome and currency data were exclusionary on a per-practice basis, resulting in 744 positions. All other trees had higher total branch lengths than 0.01137441. MEGA6 software (Tamura et al., 2013) was used for the analyses.This work aimed to create a functional nanocomposite that overcomes the antibiotic resistance of most clinical penicillin-resistant 'superbugs.' The integrated sequence from 20 isolates was sequenced and deposited in NCBI GenBank to show that *blaTEM* is prevalent. Analysis of relative species abundance and a putative resistance β-lactamase gene (Figures 11 and 12) revealed clonal dissemination of multidrug-resistant *P. aeruginosa* in the burn unit, with 100% prevalence and genetic conservation among strains from patients. This is supported by a distinct monophyletic clade in our phylogenetic analysis. Evolutionary resistance shows inadequacy: Standard β-lactam therapies are unsuccessful against these isolates due to their strong and conserved enzymatic resistance.

Molecular docking study

QM calculations: GC-MS analysis of the extract showed a range of phytochemical constituents; however, linoleic acid was selected for molecular docking simulations to study its binding affinity towards the PVA/ZnO matrix.The selection of Linoleic Acid is a key novelty of this study, as it is the first report investigating its role in stabilizing this specific nanocomposite system. Although linoleic acid constitutes only one specific fraction of the total peak area (0.5%), its selection is well-justified as an amphiphilic molecule with documented bactericidal properties. The combination of a polar carboxylic 'head' and a long hydrophobic fatty acid 'tail' gives us an interesting structural template to investigate the interfacial bonding, namely hydrogen bonding and van der Waals interactions between organic plant extract metabolites and inorganic ZnO nanoparticles. Using linoleic acid as a model ligand, this study elucidates how minor fatty acid constituents can enhance the stabilization of the nanocomposite and its inhibitory bioactivity against *Pseudomonas aeruginosa*.We performed the Density Functional Theory DFT method to calculate the molecule PVA-Linoleic acid-ZnO complex (Figure 11). The DFT computations were conducted via the Jaguar module in Schrödinger. We used an optimization tool to fine-tune our system for optimization and used the default B3LYP-D3 theory and a 6-13G basis set for

DFT, keeping the SCF spin treatment on automatic mode. We further predicted the binding mode between PVA-linoleic acid-ZnO.

Molecular docking: The 3D structure of neuraminidase was obtained from the protein data bank with accession code 4b7q. And ligand files were obtained from PubChem (https://pubchem.ncbi.nlm.nih.gov/). Ligands were prepared using molecular modeling Open Babel software (O'Boyle et al., 2011). Ligand files are saved in PDBQT format by using AutoDock. In the following step, the protein structure (PDB file) was converted into PDBQT format using AutoDockTools (ADT). The search space (grid) within the protein's active site where docking will be performed is defined. This is usually done by defining a grid box encompassing the binding site of interest. The spacing and dimensions of the grid covered the entire binding site adequately. The parameters for docking, number of runs in the genetic algorithm, population size, and maximum number of evaluations were by default (Al-Duhaidahawi et al., 2022). The default parameters guide the search algorithm in AutoDock (El-Hachem et al., 2017; Türker et al., 2020) to probe conformational space for energetically feasible binding orientations. The output files produced by AutoDock include details about the docked poses with estimated binding affinities. The output files were subsequently screened for the most favorable binding poses, as well as for estimated binding affinities of the ligands. Docking complexes were visualized using Biovia Discovery Studio (Rafi et al., 2023).

Conclusion: This study successfully combined experimental, molecular, and computational approaches to evaluate a novel ZnO/Alhagi maurorum/PVA composite film against multidrug-resistant *Pseudomonas aeruginosa* isolated from burn infections. GC-MS analysis identified several phytochemical constituents in the Alhagi extract, including linoleic acid, which may contribute to the biological activity of the composite film. The incorporation of Alhagi extract and ZnO nanoparticles into the PVA matrix resulted in enhanced antibacterial and antioxidant activities compared with the individual components. Molecular analysis confirmed the presence of *blaTEM* and *blaIMP* resistance genes among the studied isolates, while *blaTEM* amplicons were further sequenced and subjected to phylogenetic analysis. The close genetic relationship between Iraqi and international *blaTEM* sequences suggests a high degree of conservation of this resistance determinant. Computational investigations, including HOMO-LUMO analysis and molecular docking, provided additional insight into the potential interactions of the selected compounds with the investigated protein target. Although the docking results suggest favorable binding behavior, further target-specific and experimental studies are required to confirm the proposed mechanisms of action. Overall, the findings highlight the potential of ZnO/Alhagi/PVA nanocomposite films as biodegradable antimicrobial materials for future wound-dressing applications and demonstrate the value of integrating molecular epidemiology with computational approaches in antimicrobial resistance research.

Author contributions

All authors have equal contribution.

Data availability statement

The data that support the findings of this study are available from the corresponding author upon reasonable request.

Acknowledgment

Previous experts in this field did important work that made this study possible, and the author wants to thank them very much. Also, a big thank you to the College of Agriculture at Al-Qasim Green University for helping to provide and collect the samples that were needed. Also, thanks are due to the Al-Ameen Center in Al-Najaf Al-Ashraf for their help and cooperation during the study process.

Funding

The authors declare that no funds, grants, or other support were received during the preparation of this manuscript.

Ethical approval

The Faculty of Science for Women at the University of Babylon accepted the study, reference number [63], on July 14, 2025. This permission verifies that the study adhered to all the ethical criteria established by the faculty. Upon obtaining informed consent from all participants, we proceeded with the subsequent steps to protect their personal information and avert unlawful access. We ensured that all participants comprehended the prospective advantages of the trial and that the associated risks were small. Throughout the research, we adhered to all established ethical norms.

Conflict of interest

On behalf of all authors, the corresponding author states that there is no conflict of interest.

References

Abazari, M., Badeleh, S. M., Barkhordari, S., Mohammed, S. S., Ahmed, M. M., Mohammed Ameen, M. S., & Abdollahi, H. (2025). Preparation and characterization of polyvinyl alcohol thin films: Rheological, physicochemical and functional properties. *Heliyon*, *11*(12), Article e43604. https://doi.org/10.1016/j.heliyon.2025.e43604

Abdelrazek, E. M., Elashmawi, I. S., & Labeeb, S. (2010). Chitosan filler effects on the experimental characterization, spectroscopic investigation and thermal studies of PVA/PVP blend films. *Physica B: Condensed Matter*, *405*(8), 2021-2027. https://doi.org/10.1016/j.physb.2010.01.095

Abdelrazek, E. M., Abdelghany, A. M., & Tarabiah, A. E. (2019). AC conductivity and dielectric characteristics of PVA/PVP nanocomposite filled with MWCNTs. *Journal of Materials Science: Materials in Electronics*, *30*, 15521-15533. https://doi.org/10.1007/s10854-019-01929-2

Abdulbary, M. (2019). Study of some properties and antibacterial activity of (*Alhagi maurorum* Medik) collected from the desert of Al-Najaf. *Journal of Physics: Conference Series*, *1294*, Article 062081. https://doi.org/10.1088/1742-6596/1294/6/062081

Ahmed, S., Ahmad, M., Swami, B. L., & Ikram, S. (2016). A review on plants extract mediated synthesis of silver nanoparticles for antimicrobial applications: A green expertise. *Journal of Advanced Research*, *7*(1), 17-28. https://doi.org/10.1016/j.jare.2015.02.007

Al-Duhaidahawi, D., Al-Zubaidy, H. F. S., Al-Khafaji, K., & Al-Amiery, A. (2022). Synthesis, anti-inflammatory effects, molecular docking and molecular dynamics studies of 4-

hydroxy coumarin derivatives as inhibitors of COX-II enzyme. *Journal of Molecular Structure*, *1247*, Article 131377. https://doi.org/10.1016/j.molstruc.2021.131377

Al-Snafi, A. (2015). *Alhagi maurorum* as a potential medicinal herb: An overview. *International Journal of Pharmacy Review and Research*, *5*, 130-136.

Asadpour, S., Raeisi vanani, A., Kooravand, M., & Asfaram, A. (2022). A review on zinc oxide/poly(vinyl alcohol) nanocomposites: Synthesis, characterization and applications. *Journal of Cleaner Production*, *362*, Article 132297. https://doi.org/10.1016/j.jclepro.2022.132297

Barbălată-Mândru, M., Serbezeanu, D., Butnaru, M., Rîmbu, C. M., Enache, A. A., & Aflori, M. (2022). Poly(vinyl alcohol)/plant extracts films: Preparation, surface characterization and antibacterial studies against Gram positive and Gram negative bacteria. *Materials*, *15*(7), Article 2493. https://doi.org/10.3390/ma15072493

Benson, D. A., Cavanaugh, M., Clark, K., Karsch-Mizrachi, I., Lipman, D. J., Ostell, J., & Sayers, E. W. (2013). GenBank. *Nucleic Acids Research*, *41*(D1), D36-D42. https://doi.org/10.1093/nar/gks1195

Brzęk, P., & Sterzyński, T. (2020). Stress whitening as an observation method of residual stress in MABS polymer material through the example of holding pressure in an injection molding process. *Polymers*, *12*(12), Article 2871. https://doi.org/10.3390/polym12122871

Bush, K., & Bradford, P. A. (2020). Epidemiology of β-lactamase-producing pathogens. *Clinical Microbiology Reviews*, *33*(2), Article e00047-19. https://doi.org/10.1128/CMR.00047-19

Castanheira, M., Simner, P. J., & Bradford, P. A. (2021). Extended-spectrum β-lactamases: An update on their characteristics, epidemiology and detection. *JAC-Antimicrobial Resistance*, *3*(3), Article dlab092. https://doi.org/10.1093/jacamr/dlab092

Eftekhari, F., Sarcheshmehpour, M., Lohrasbi-Nejad, A., & Boroomand, N. (2025). Effects of mycorrhizal and *Trichoderma* treatment on enhancing maize tolerance to salinity and drought stress, through metabolic and enzymatic evaluation. *BMC Plant Biology*, *25*(1), Article 687. https://doi.org/10.1186/s12870-025-06729-x

El-Hachem, N., Haibe-Kains, B., Khalil, A., Kobeissy, F. H., & Nemer, G. (2017). AutoDock and AutoDockTools for protein-ligand docking: Beta-site amyloid precursor protein cleaving enzyme 1 (BACE1) as a case study. *Methods in Molecular Biology*, *1598*, 391-403. https://doi.org/10.1007/978-1-4939-6952-4_20

Franco, D., Calabrese, G., Guglielmino, S. P. P., & Conoci, S. (2022). Metal-based nanoparticles: Antibacterial mechanisms and biomedical application. *Microorganisms*, *10*(9), Article 1778. https://doi.org/10.3390/microorganisms10091778

Ghasemi, H., Omranifard, M., Bahrami, M., Moghimian, M., & Farzi, S. (2025). Challenges in burn care management: A qualitative study of health professionals' and patients' perspectives. *Scientific Reports*, *15*(1), Article 33401. https://doi.org/10.1038/s41598-025-18722-3

Gulcin, İ., & Alwasel, S. H. (2023). DPPH radical scavenging assay. *Processes*, *11*(8), Article 2248. https://doi.org/10.3390/pr11082248

Hakeem, H. S., Muhsen, M. F., & Taieh, N. K. (2024). Optical characterization of polyvinyl alcohol-zinc oxide nanocomposite films fabricated via spray coating and enhanced through plasma modification: A comprehensive study. *Journal of Nanotechnology*, *2024*, Article 8878626. https://doi.org/10.1155/jnt/8878626

Heidarpour, F., Mohammadabadi, M. R., Zaidul, I. S. M., Maherani, B., Saari, N., Hamid, A. A., Abas, F., Manap, M. Y. A., & Mozafari, M. R. (2011). Use of prebiotics in oral delivery of bioactive compounds: A nanotechnology perspective. *Pharmazie*, *66*(5), 319-324.

Hussein, A. A., Kaddim Radi, N., & Mohammed Sahi, N. (2025). Integrative computational and experimental study of propolis, polyvinyl alcohol, and *Alhagi maurorum* complex as anticancer and antibacterial agents. *Journal of Biomaterials Science, Polymer Edition*, *36*(12), 1718-1748. https://doi.org/10.1080/09205063.2025.2464448

Ibrahim, S., Al-Dahir, S., Al Mulla, T., Lami, F., Hossain, S. M. M., Baqui, A., & Burnham, G. (2021). Resilience of health systems in conflict affected governorates of Iraq, 2014-2018. *Conflict and Health*, *15*(1), Article 76. https://doi.org/10.1186/s13031-021-00412-2

Jabalia, N., Kumar, A., Kumar, V., & Rani, R. (2021). In silico approach in drug design and drug discovery: An update. In S. K. Singh (Ed.), *Innovations and implementations of computer aided drug discovery strategies in rational drug design* (pp. 1-28). Springer. https://doi.org/10.1007/978-981-15-8936-2_10

Liang, X., Zhong, H.-J., Ding, H., Yu, B., Ma, X., Liu, X., Chong, C.-M., & He, J. (2024). Polyvinyl alcohol (PVA)-based hydrogels: Recent progress in fabrication, properties, and multifunctional applications. *Polymers*, *16*(19), Article 2755. https://doi.org/10.3390/polym16192755

Mostafa, R. M., & Essawy, H. S. (2019). Assessment of camel thorn (*Alhagi maurorum*) as new sources of bioactive compounds using GC-MS technique. *Plant Omics*, *12*(1), 70-76.

Muhammad, M., Waheed, A., Wahab, A., Majeed, M., Nazim, M., Liu, Y.-H., Li, L., & Li, W.-J. (2024). Soil salinity and drought tolerance: An evaluation of plant growth, productivity, microbial diversity, and amelioration strategies. *Plant Stress*, *11*, Article 100319. https://doi.org/10.1016/j.stress.2023.100319

Nandy, S., Das, A. K., & Dudeja, M. (2017). Prevalence of metallo beta lactamase in clinical isolates of *Pseudomonas aeruginosa* in a tertiary care hospital. *International Journal of Community Medicine and Public Health*, *2*(4), 566-569. https://doi.org/10.18203/2394-6040.ijcmph20151048

O'Boyle, N. M., Banck, M., James, C. A., Morley, C., Vandermeersch, T., & Hutchison, G. R. (2011). Open Babel: An open chemical toolbox. *Journal of Cheminformatics*, *3*, Article 33. https://doi.org/10.1186/1758-2946-3-33

Oliver, A., Arca-Suárez, J., Gomis-Font, M. A., González-Pinto, L., López-Causapé, C., & Others. (2025). Emerging resistance mechanisms to newer β-lactams in *Pseudomonas aeruginosa*. *Clinical Microbiology and Infection*, *31*(11), 1790-1796. https://doi.org/10.1016/j.cmi.2025.03.013

Premkumar, H. (2024). Synthesis, characterization and photocatalytic performance of polyvinyl alcohol/zinc oxide nanocomposites: A comprehensive study. *Nano-Structures & Nano-Objects*, *39*, Article 101208. https://doi.org/10.1016/j.nanoso.2024.101208

Qin, S., Xiao, W., Zhou, C., Pu, Q., Deng, X., Lan, L., Liang, H., Song, X., Wu, M., & Others. (2022). *Pseudomonas aeruginosa*: Pathogenesis, virulence factors, antibiotic resistance, interaction with host, technology advances and emerging therapeutics. *Signal Transduction and Targeted Therapy*, *7*(1), Article 199. https://doi.org/10.1038/s41392-022-01056-1

Radi, N. K., & Al-Marzoqi, A. H. (2022). Detection of virulent genetic markers like blaTEM, blaIMP1 of pathogenic *E. coli* strain isolated from Iraqi frozen chicken meat. *International Journal of Health Sciences*, *6*(S1), 6864-6874. https://doi.org/10.53730/ijhs.v6nS1.6679

Rafi, M. O., Al-Khafaji, K., Mandal, S. M., Meghla, N. S., Biswas, P. K., Rahman, M. S., & Others. (2023). A subunit vaccine against pneumonia: Targeting *Streptococcus pneumoniae* and *Klebsiella pneumoniae*. *Network Modeling Analysis in Health Informatics and Bioinformatics*, *12*(1), Article 21. https://doi.org/10.1007/s13721-023-00416-3

Saber, T. M., Abo-Elmaaty, A. M. A., Said, E. N., Beheiry, R. R., Moselhy, A. A., Abdelgawad, F. E., Arisha, M. H., Saber, T., Arisha, A. H., & Fahmy, E. M. (2022). *Alhagi maurorum* ethanolic extract rescues hepato-neurotoxicity and neurobehavioral alterations induced by lead in rats via abrogating oxidative stress and the caspase-3-dependent apoptotic pathway. *Antioxidants*, *11*(10), Article 1992. https://doi.org/10.3390/antiox11101992

Sabr, O. H., Obaid, M. N., Al-Mutairi, N. H., Krynke, M., & Mielczarek, K. (2024). Study the effect of zinc oxide nanoparticles on degradation, antibacterial, thermal and morphological properties of polyvinyl alcohol films. *Production Engineering Archives*, *30*(4), 528-536. https://doi.org/10.30657/pea.2024.30.49

Shalmashi, H., Farajnia, S., Sadeghi, M., Tanoumand, A., Veissi, K., Hamishekar, H., & Gotaslou, R. (2022). Detection of ESBLs types blaCTX-M, blaSHV and *blaTEM* resistance

genes among clinical isolates of *Pseudomonas aeruginosa*. *Gene Reports*, *28*, Article 101637. https://doi.org/10.1016/j.genrep.2022.101637

Singh, S., Sahoo, R. K., & Sahu, M. C. (2025). Understanding recent developments in colistin resistance: Mechanisms, clinical implications, and future perspectives. *Antibiotics*, *14*(10), Article 958. https://doi.org/10.3390/antibiotics14100958

Sirelkhatim, A., Mahmud, S., Seeni, A., Kaus, N. H. M., Ann, L. C., Bakhori, S. K. M., Hasan, H., & Mohamad, D. (2015). Review on zinc oxide nanoparticles: Antibacterial activity and toxicity mechanism. *Nano-Micro Letters*, *7*, 219-242. https://doi.org/10.1007/s40820-015-0040-x

Tacconelli, E., Carrara, E., Savoldi, A., Harbarth, S., Mendelson, M., Monnet, D. L., Pulcini, C., Kahlmeter, G., Kluytmans, J., Carmeli, Y., Ouellette, M., Outterson, K., Patel, J., Cavaleri, M., Cox, E. M., Houchens, C. R., Grayson, M. L., Hansen, P., Singh, N., ... Magrini, N. (2018). Discovery, research, and development of new antibiotics: The WHO priority list of antibiotic-resistant bacteria and tuberculosis. *The Lancet Infectious Diseases*, *18*(3), 318-327. https://doi.org/10.1016/S1473-3099(17)30753-3

Tamura, K., Stecher, G., Peterson, D., Filipski, A., & Kumar, S. (2013). MEGA6: Molecular Evolutionary Genetics Analysis version 6.0. *Molecular Biology and Evolution*, *30*(12), 2725-2729. https://doi.org/10.1093/molbev/mst197

Türker, F., Noma, S. A. A., Aktaş, A., Al-Khafaji, K., Taşkın Tok, T., Ateş, B., & Gök, Y. (2020). The (NHC)$PdBr_2$(2-aminopyridine) complexes: Synthesis, characterization, molecular docking study, and inhibitor effects on the human serum carbonic anhydrase and serum bovine xanthine oxidase. *Monatshefte für Chemie - Chemical Monthly*, *151*, 1557-1567. https://doi.org/10.1007/s00706-020-02687-2

Udayagiri, H., Sana, S. S., Dogiparthi, L. K., Vadde, R., Varma, R. S., Koduru, J. R., Ghodake, G. S., Somala, A. R., Boya, V. K. N., Kim, S. C., & Karri, R. R. (2024). Phytochemical fabrication of ZnO nanoparticles and their antibacterial and anti-biofilm activity. *Scientific Reports*, *14*(1), Article 19714. https://doi.org/10.1038/s41598-024-69044-9

Vasile, C., & Baican, M. (2021). Progresses in food packaging, food quality, and safety—Controlled-release antioxidant and/or antimicrobial packaging. *Molecules*, *26*(5), Article 1263. https://doi.org/10.3390/molecules26051263

Wen, Y. H., Tsou, C. H., de Guzman, M. R., Huang, D., Yu, Y. Q., Gao, C., Zhang, X. M., Du, J., Zheng, Y. T., Zhu, H., & Wang, Z. H. (2022). Antibacterial nanocomposite films of poly(vinyl alcohol) modified with zinc oxide-doped multiwalled carbon nanotubes as food packaging. *Polymer Bulletin*, *79*, 3847-3866. https://doi.org/10.1007/s00289-021-03666-1

Wong, T. T., Amigues, S., & Awaja, F. (2025). The influence of zinc oxide nanoparticles on dispersion, rheology, and mechanical properties of epoxy-based composites. *Polymers*, *17*(24), Article 3253. https://doi.org/10.3390/polym17243253

Xie, Y., Cai, P., Cao, X., Chen, B., & Pan, Y. (2024). Water-resistant poly(vinyl alcohol)/ZnO nanopillar composite films for antibacterial packaging. *ACS Omega*, *9*(51), 50403-50413. https://doi.org/10.1021/acsomega.4c07173

Yue, Y., Cheng, X., Liu, H., Zang, M., Zhao, B., Zhao, X., & Wang, L. (2023). Gellan gum and polyvinyl alcohol based triple-layer films enriched with *Alhagi sparsifolia* flower extract: Preparation, characterization, and application of dried shrimp preservation. *Foods*, *12*(21), Article 3979. https://doi.org/10.3390/foods12213979

Zarrabi, A., Alipoor Amro Abadi, M., Khorasani, S., Mohammadabadi, M., Jamshidi, A., Torkaman, S., Taghavi, E., Mozafari, M. R., & Rasti, B. (2020). Nanoliposomes and tocosomes as multifunctional nanocarriers for the encapsulation of nutraceutical and dietary molecules. *Molecules*, *25*(3), Article 638. https://doi.org/10.3390/molecules25030638

مجله بیوتکنولوژی کشاورزی
شاپا چاپی: ۶۷۰۵-۲۲۲۸ شاپا الکترونیکی: ۶۵۰۰-۲۲۲۸

ارزیابی تجربی و درون‌سیلیکویی (In Silico) یک فیلم کامپوزیتی نوین ZnO/Alhagi maurorum/PVA علیه سویه‌های مقاوم به چند دارو از *Pseudomonas aeruginosa* حامل ژن‌های *blaTEM* و blaIMP

نسرین کاظم راضی
گروه زیست‌شناسی، دانشکده علوم برای بانوان، دانشگاه بابل، عراق. ایمیل: nesreenzain.83@gmail.com و Nasreen.radi@uobabylon.edu.iq

شیرین صباح کامل
گروه زیست‌شناسی، دانشکده علوم برای بانوان، دانشگاه بابل، عراق. ایمیل: Shireensbahkamil@gmail.com

صفا حسن راضی
گروه زیست‌شناسی، دانشکده علوم، دانشگاه سبز القاسم، بابل ۵۱۰۱۳، عراق. ایمیل: safa.safa252016@gmail.com

حسین ج. حسین
گروه زیست‌شناسی، دانشکده علوم برای بانوان، دانشگاه بابل، عراق. ایمیل: huss2010feb@yahoo.com

علی ه. المرزوقی
گروه زیست‌شناسی، دانشکده علوم برای بانوان، دانشگاه بابل، عراق. ایمیل: almarzoqiali80@gmail.com

لبنی عبدالعظیم
مرکز تحقیقات DNA، دانشگاه بابل، عراق. ایمیل: sci.lubna.addeladeem@uobabylon.edu.iq

اسراء ا. ابراهیم
گروه زیست‌شناسی، دانشکده علوم برای بانوان، دانشگاه بابل، عراق. ایمیل: israaibraheam2016@gmail.com

علی سلام کشکول
دانشگاه فنی میانه، مؤسسه فنی کوت، عراق. ایمیل: alimayhie11@gmail.com

تاریخ دریافت: ۱۴۰۵/۰۱/۲۴ تاریخ دریافت فایل اصلاح شده نهایی: ۱۴۰۵/۰۳/۲۹ تاریخ پذیرش: ۱۴۰۵/۰۳/۳۰

چکیده

هدف: باکتری *سودوموناس آئروژینوزا* یکی از عوامل اصلی عفونت‌های ناشی از سوختگی است که به دلیل بیماری‌زایی بالا و مقاومت دارویی شناخته می‌شود. این مطالعه با هدف تهیه و مشخصه‌یابی فیلم نانوکامپوزیتی ZnO/PVA حاوی عصاره گیاه *Alhagi maurorum* برای مقابله با سویه‌های مقاوم به چند دارو از *P. aeruginosa* جداشده از عفونت‌های پوستی ناشی از سوختگی

انجام شد. همچنین شناسایی مولکولی و تعیین توالی ژن‌های *blaTEM* و *blaIMP* و به دنبال آن تحلیل اتصال مولکولی درون‌سیلیکویی به منظور بررسی مکانیسم ضدباکتریایی انجام گرفت.

مواد و روش‌ها: سرشاخه‌های گیاه *Alhagi maurorum* جمع‌آوری و نمونه‌های شاهد نگهداری شدند. آنالیز GC-MS بر روی عصاره گیاهی انجام شد. نانوذرات اکسید روی در ماتریس پلیمری به کار گرفته شدند. ارزیابی‌های جامعی برای تأیید به‌دام‌افتادن موفق و توزیع یکنواخت نانوترکیبات زیست‌فعال در ماتریس پلیمری فیلم کامپوزیتی ساخته‌شده انجام شد. تعداد ۵۰ جدایه باکتریایی از سواب‌های بیماران بستری در بخش سوختگی بیمارستان به دست آمد. حساسیت ضدمیکروبی جدایه‌های *P. aeruginosa* (۲۰ جدایه) تعیین شد. DNA ژنومی از جدایه‌های باکتریایی استخراج و PCR انجام گردید. توالی‌های نوکلئوتیدی ژن *blaTEM* مربوط به *P. aeruginosa* از پایگاه NCBI استخراج شد. برای تجزیه و تحلیل آماری از نرم‌افزار SPSS استفاده گردید.

نتایج: نتایج GC-MS نشان داد که طیف جرمی و ساختار دوازده ترکیب شیمیایی استخراج‌شده از گیاه *Alhagi maurorum* با استفاده از متانول در داده‌های GC-MS قابل مشاهده است. در میان این ترکیبات، اسید ۹،۱۲-اکتادکادی‌انوئیک (Z,Z) (اسید لینولئیک) از ویژگی خاصی برخوردار بود. با ترکیب این مواد فیتوشیمیایی در ماتریس پلیمری PVA همراه با نانوذرات روی، فیلمی زیست‌تخریب‌پذیر تولید شد. این فیلم در برابر جدایه‌های بالینی *Pseudomonas aeruginosa* که دارای مقاومت دارویی بودند، مورد آزمایش قرار گرفت. از میان ۵۰ جدایه باکتریایی، ۲۰ جدایه به عنوان *P. aeruginosa* شناسایی شدند. نتایج PCR وجود ژن‌های *blaTEM* و *blaIMP* را در درصد قابل توجهی از جدایه‌ها نشان داد. نتایج داکینگ مولکولی حاکی از آن بود که نانوساختار ZnO در مقایسه با اسید لینولئیک و PVA بیشترین توانایی اتصال به پروتئین را دارد. میل اتصال قوی و ثابت مهاری پایین ZnO نقش بالقوه آن را به عنوان یک متصل‌شونده یا مهارکننده پایدار نشان می‌دهد، در حالی که اسید لینولئیک و PVA کارایی کمتری داشتند.

نتیجه‌گیری: خواص ضدباکتریایی قوی این فیلم کامپوزیتی احتمالاً حاصل اثر هم‌افزای پلیمر PVA، نانوذرات روی و عصاره گیاهی است. فیلم کامپوزیتی ZnO/Alhagi/PVA فعالیت‌های ضدباکتریایی و آنتی‌اکسیدانی امیدبخشی از خود نشان داد و می‌تواند به عنوان یک ماده زیست‌تخریب‌پذیر بالقوه برای پانسمان زخم در مدیریت عفونت‌های ناشی از *P. aeruginosa* مقاوم به چند دارو مورد استفاده قرار گیرد.

کلمات کلیدی: بتالاکتاماز، پلی‌وینیل الکل (PVA)، فیلم‌های ضدباکتریایی، نانوذرات روی، *Alhagi maurorum*

نوع مقاله: پژوهشی

استناد: نسرین کاظم راضی، شیرین صباح کامل، صفا حسن راضی، حسین ج. حسین، علی ه. المرزوقی، لبنی عبدالعظیم، اسراء ا. ابراهیم، علی سلام کشکول (۱۴۰۵). ارزیابی تجربی و درون‌سیلیکویی (In Silico) یک فیلم کامپوزیتی نوین ZnO/Alhagi maurorum/PVA علیه سویه‌های مقاوم به چند دارو از *Pseudomonas aeruginosa* حامل ژن‌های *blaTEM* و blaIMP. *مجله بیوتکنولوژی کشاورزی*، ۱۸(۴)، ۳۳۹-۳۷۲.

Publisher: Shahid Bahonar University of Kerman & Iranian Biotechnology Society.